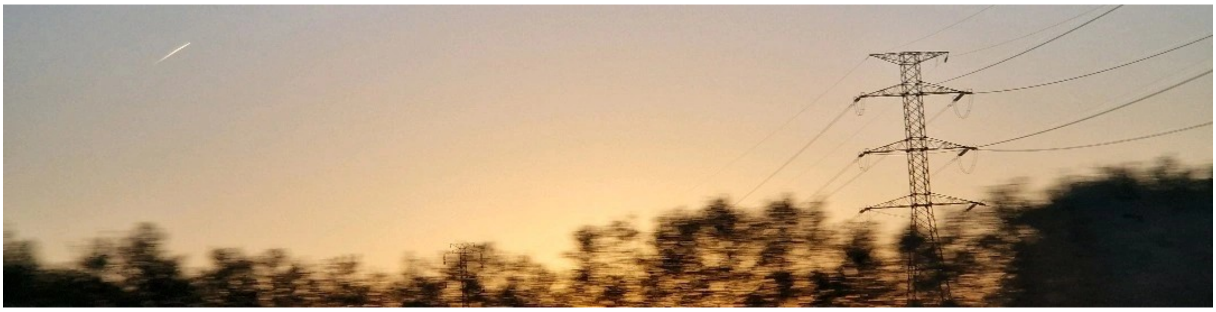

Voltage Control Interactions in Active Distribution Networks: A Stability Analysis Approach for Piecewise-Linear Local Control Laws

Tomás Gomes Glória

Thesis to obtain the Master of Science Degree in

Electrical and Computer Engineering

Supervisors: Prof. Pedro Manuel Santos de Carvalho
Dr. Diogo Manuel dos Santos Vilela Pinto Ferreira

Examination Committee

Chairperson: Prof. Célia Maria Santos Cardoso de Jesus
Supervisor: Prof. Pedro Manuel Santos de Carvalho
Member of the Committee: Prof. Hugo Gabriel Valente Morais

December 2025

Há vitórias e derrotas
Apontadas em silêncio
No diário imaginário
Onde empilhamos as razões para lutar

— Jorge Palma

Declaration

I declare that this document is an original work of my own authorship and that it fulfills all the requirements of the Code of Conduct and Good Practices of the Universidade de Lisboa.

Agradecimentos

Em primeiro lugar, gostaria de agradecer a todos os meus amigos com quem partilhei a jornada no Técnico. Cada um de vocês foi imprescindível para que nunca me sentisse sozinho e para que, todas as manhãs, ao chegar ao Técnico, sentisse que estava a chegar a casa. Tiago, Faria, Frazão, Tomás, Afonso, Maria, Leo, Costa, Diogo e Taquito, obrigado. Aos amigos fora do Técnico, obrigado por todos os momentos de alegria e felicidade, Rodrigo, Cath, Cortes, Dani, Gonçalo, Miguel, Pedro, Vasco, Yuri e Rodolfo, obrigado.

Gostaria também de agradecer a todos os professores do Técnico com quem tive o privilégio de aprender. Obrigado por transmitirem sempre o vosso entusiasmo pela Engenharia Eletrotécnica e de Computadores. Em particular, agradeço ao Professor Hugo Morais, por me ter aberto as portas à investigação e pela oportunidade de aprender ainda mais na área que mais me apaixona.

Um grande agradecimento aos meus orientadores. Ao Professor Pedro Carvalho, obrigado por ter tornado tão clara a minha vontade de seguir a área da energia, através das aulas formidáveis de Fundamentos de Energia Elétrica e das restantes cadeiras do mestrado. Obrigado também pelos seus conselhos valiosos, pelo apoio contínuo e pela constante disponibilidade. A sua descontração, e o profundo conhecimento, serão sempre uma inspiração para mim. Ao recém-doutor Diogo, obrigado por teres acreditado em mim desde o início até ao fim. A tese foi um caminho longo e difícil, mas sempre que a cabeça baixava podia contar com a tua voz experiente para me ajudar a seguir em frente. Obrigado também pela tua voz de amigo, para além de orientador.

Aos Beatles, Pink Floyd e Bob Dylan, obrigado pela música.

Por fim, agradeço a toda a minha família, o pilar fundamental sobre o qual construo a minha vida com confiança. Ao Benji e ao Oliver obrigado pela companhia. Obrigado a minha tia Zea e prima Joana. À prima Carolina, obrigado por teres sido a melhor primeira colega de casa possível, por me teres apresentado à vida em Lisboa e ao Técnico. Ao avô Jorge e à avó Graciete, obrigado pela humildade e amor que me passam. À avó Anita e ao avô António, obrigado por me ensinarem a viver a vida de forma tão alegre e pelo amor que sempre me transmitem. A ti, Meti, obrigado por seres a amiga de uma vida. Teres nascido sob as mesmas asas que eu foi a minha sorte grande. Ao meu papá, Zé, obrigado pelo amor e por teres construído o berço de ouro onde nasci e cresci. O teu bom humor e a tua disciplina no trabalho moldaram muito daquilo que sou. À minha mamã, Ana Gabi, obrigado por seres uma super mulher e uma super super mãe. Nada me inspira tanto como a tua força aliada ao sorriso constante e à forma feliz como olhas para a vida. Obrigado por me passares tudo isso com tanto amor.

Abstract

Voltage control devices are expected to operate autonomously in active distribution networks according to piecewise-linear control laws as established by EU regulations and IEEE standards. Therefore, to preserve normal operating conditions, network supervisors need to guarantee that the interactions that result from the actuation between these control laws are stable. Yet, stability analysis approaches found in the literature narrow the analysis of local controllers to linear control laws with slopes alone. This thesis proposes a new piecewise-linear state-space model that can be used for stability analysis of local controllers, expanding control laws to have slopes, dead- and saturation zones. The proposed model makes use of a robust simulation approach, based on reachable sets theory, to analyse the stability of voltage control interactions. Proof is also provided that Lyapunov-based approaches offer limited insights into the stability of piecewise-linear control laws, matching the results found with small-signal stability analysis for linear control laws. Results illustrate the advantages of the proposed approach over Lyapunov and small-signal stability approaches for low voltage distribution networks.

Keywords

Active distribution networks, active distribution system management, local control, piecewise linear state-space model, stability analysis.

Resumo

Os dispositivos de controlo de tensão deverão operar de forma autónoma em redes de distribuição ativas, seguindo leis de controlo lineares por troços, conforme estabelecido pelos regulamentos da União Europeia e pelas normas IEEE. Para preservar as condições normais de operação, os supervisores da rede devem garantir que as interações resultantes entre essas leis de controlo sejam estáveis. No entanto, a literatura existente sobre análise de estabilidade limita-se, em grande parte, a controladores locais com leis de controlo estritamente lineares. Esta tese apresenta um novo modelo de espaço de estado linear por partes, desenvolvido para a análise de estabilidade de controladores locais. O modelo proposto permite estender as leis de controlo de forma a incluir inclinações, zonas mortas, e zonas de saturação. A análise de estabilidade é realizada através de uma abordagem de simulação robusta baseada na teoria de *reachable sets*. Adicionalmente, a tese demonstra que as abordagens baseadas na teoria de Lyapunov fornecem uma perspetiva limitada sobre a estabilidade das leis de controlo lineares por partes, corroborando os resultados obtidos com a análise small-signal para leis de controlo lineares. Os resultados evidenciam as vantagens da metodologia proposta em comparação com os métodos tradicionais de estabilidade de Lyapunov aplicados a redes de distribuição.

Palavras Chave

Redes de distribuição ativas, gestão ativa do sistema de distribuição, controlo local, modelo de espaço de estado linear por partes, análise de estabilidade.

Contents

List of Figures

List of Tables

Acronyms

ADN	active distribution network
CQLF	common quadratic Lyapunov function
DER	distributed energy resources
DN	distribution network
DSO	distribution system operator
FACTS	flexible AC transmission systems
LMI	linear matrix inequality
LTI	linear time invariant
LV	low voltage
OLTC	on-load tap changer
PV	photovoltaic
PWA	picewiese affine
PWQLF	piecewise quadratic Lyapunov function
QLF	quadratic Lyapunov function
RfG	Requirements for Generators
SOP	Soft Open Points
STATCOM	static condenser
SVC	static VAr compensator
VC	voltage controller

1

Introduction

Contents

This chapter provides a brief overview of the problem addressed in this thesis. It begins with a motivation that connects the challenges of climate change to the growing need for active control in distribution networks (DNs), illustrated by the recent blackout event of April 2025. The chapter then presents the main objectives of the work and the research gap it aims to address. Finally, the structure and outline of the thesis are introduced.

1.1 Motivation

For millennia, human beings lived as hunter-gatherers, dependent on the environment and subject to its constraints. As with other species, their capacity to influence the course of the Earth climate was limited. The formation of social groups, such as tribes and early communities, signified a pivotal transition, propelling humans towards enhanced collective efficacy and exerting a growing influence over their ecosystems. While the transition to settled societies and agriculture represented a gradual process of increasing human control over nature, the Industrial Revolution marked a significant turning point. The substantial utilization of fossil fuels, in conjunction with rapid advancements in technology, has enabled humanity to exert a previously unparalleled degree of influence over the planet's evolution [1]. From this period onward, human activity became a central factor in shaping environmental processes. The intensive extraction and combustion of fossil fuels introduced vast quantities of greenhouse gases into the atmosphere, initiating a trajectory of global climate change that has continued to accelerate into the present day [2].

1.1.1 The Effect of Greenhouse Gases on Climate Change

Greenhouse gases play a fundamental role in maintaining Earth's temperature by trapping part of the outgoing infrared radiation emitted from the planet's surface. Without this natural greenhouse effect, most of the radiation would escape into space, and average global temperatures would be far too low to sustain human life as it exists today. However, the rapid increase in greenhouse gas concentrations resulting from human activities has disrupted this balance. As it is evident in Figure 1.1 the increase in greenhouse emissions is increasing the temperature of the planet, driving global warming and associated environmental changes [3].

The adverse effects of climate change have led to a global awareness of the issue. In 1992, this awareness prompted the first significant action by humankind to address climate change: the Earth Summit in Rio de Janeiro. This summit is regarded as a landmark moment in the field of global environmental governance, as it established a comprehensive framework for sustainable development by integrating environmental protection with economic and social progress [5]. After the Rio Summit, the UNFCCC framework was strengthened by two major agreements. The Kyoto Protocol, adopted in 1997,

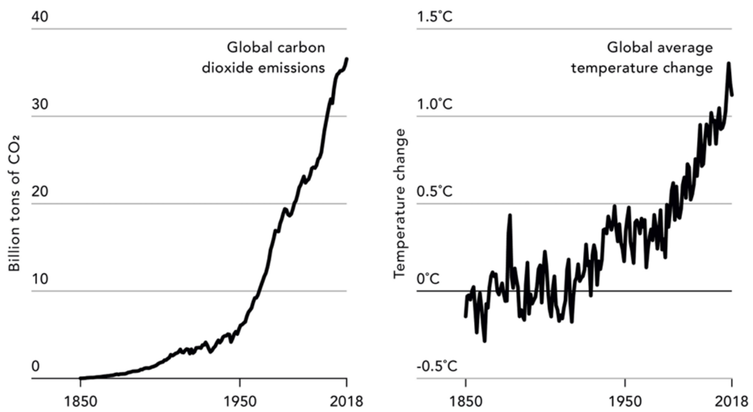

Figure 1.1: Carbon dioxide emissions and global average temperature since 1850. Figure extracted from [4].

introduced binding emission reduction targets for developed countries [6]. Later, the Paris Agreement of 2015 established a universal commitment, with all nations pledging nationally determined contributions to limit global warming to below 2 ºC, and to pursue efforts toward 1.5 ºC [7].

1.1.2 The Paradigm Shift in the Energy Sector

There are several sectors of human activity that contribute significantly to environmental degradation, each in different ways. Among these, the energy sector stands out as the largest source of greenhouse gas emissions, primarily due to the reliance on fossil fuels such as coal, oil, and natural gas for electricity generation. In 2010, this sector alone accounted for approximately 35% of global greenhouse gas emissions, underscoring its central role in driving climate change [8]. Moreover, the growing demand for energy in both developed and emerging economies has intensified pressure on this sector, making it a focal point for climate mitigation strategies. Transitioning the energy sector toward low-carbon and renewable sources is therefore considered one of the most critical challenges in achieving global sustainability goals. Nevertheless, achieving a decarbonized energy sector necessitates more than a mere transition in primary energy sources. The replacement of fossil fuels with carbon-neutral alternatives, such as wind, hydropower, and solar energy, is a pivotal component of this transition. However, the efficacy of this solution is contingent upon the electrification of end-use sectors, including households, transportation, and industry [9]. Beyond generating clean, emission-free power and using it through electrified means, a strong and reliable structure is needed to connect the two: the electrical networks, which serves as the backbone of the energy transition and ensures that sustainable generation can effectively meet modern electricity demands. Yet, the evolving paradigm of generating and consuming electric energy raise the question of whether the traditional planning and operation of power networks will remain adequate from a cost-effective perspective [9].

Yesterday, all DNs problems seemed so far away, now its looks as though they're here to stay. Historically, DNs were designed under the assumption of unidirectional, top-down power flows, with most operational challenges addressed during the planning stage by sizing equipment to meet peak load demand. Nonetheless, these conventional assumptions are no longer valid as a growing share of end-user demand is supplied by generation located at the distribution level. Distributed Generation is found not to match exactly the local consumption needs, leading to situations where injections exceed demand and reverse power flows occur. At the same time, the rapid uptake of new electrified equipments like electric vehicles and heat pumps can create demand surges that strain existing and planned network capacity [10]. Together, these dynamics result in high net-load volatility and more frequent bidirectional flows, which introduce new operational challenges such as network congestion, undervoltages and overvoltages that were not accounted for in traditional planning approaches [11]. Therefore, in order to ensure the security of network operations in a manner that is both effective and economical, distribution system operator (DSO) must adapt and implement new strategies that place a greater emphasis on operational processes. The necessity for novel operational solutions that depend on the actuation of control devices and network monitoring is growing, as these solutions are imperative in preserving normal operating conditions [12, 13].

The integration of dynamic control devices, such as smart inverters, has emerged as a promising solution. Since photovoltaic (PV) installations are typically coupled with smart inverters, the growing deployment of distributed energy resources (DER) inherently increases the availability of voltage control resources. Smart inverters are capable of providing reactive power compensation and activate power adjustment, thereby alleviating the switching burden on traditional devices and enhancing voltage profiles in networks with high levels of intermittent generation [14]. Yet, with great power comes great responsibility as the increasing availability of control devices will bring new challenges to the operation of active distribution network (ADN). Namely, as each devices focus only on its own objectives, the interactions between each other, potentially driving the network toward unstable behavior. To mitigate these risks, the EU and IEEE have established regulations and standards that such devices must follow. Consequently, network operators must have access to tools capable of ensuring system stability while coordinating the operation of these devices in accordance with the prescribed control curves.

1.1.3 The 2025 Iberian Blackout

On April 28, 2025, the Iberian Peninsula witnessed a blackout of unprecedented magnitude, the most severe incident in the European power system for over two decades. According to ENTSO-E and the respective transmission system operators, the event originated from a sequence of disturbances that ultimately led to a widespread loss of synchronism and cascading disconnections. The investigation identified several contributing factors, including voltage oscillations, over-voltage phenomena, and insufficient reactive power support under stressed system conditions. The incident has highlighted once again the critical importance of voltage stability for the secure operation of modern power systems.

According to the factual report published by ENTSO-E regarding the aforementioned blackout [15], two distinct periods of oscillation were identified in the Continental Europe Synchronous Area during the half-hour period preceding the blackout. In order to mitigate these oscillations, the operators in the control rooms of the relevant TSOs implemented several mitigating measures, such as reducing the export from Spain to France. Although these measures served to mitigate the oscillations, their inherent characteristics resulted in an increase in the voltage of the Iberian power system. A series of generator disconnections across several Spanish regions exposed significant limitations in the voltage support mechanisms of the transmission system. The initial loss of distributed wind and solar generation led to local voltage increases that were not effectively mitigated by existing control and protection schemes. Although the recorded voltage levels (approximately 418–435 kV at 400 kV nominal) were not extreme, multiple renewable facilities disconnected instead of providing reactive power support. As some generation units were consuming reactive power, with the effect of reducing the voltage, the disconnections of these units without adequate compensation for the loss of reactive power by other resources in the system, with the capability to inject/absorb reactive power, meant that voltages in the system increased, not only in Spain but also in Portugal. Furthermore, the frequency decreased. The electrical separation of the Iberian system was completed by the tripping of the HVDC lines that transmitted power from Spain to France, and all system parameters of the Spanish and Portuguese electricity systems collapsed.

Several changes in operational regulations were implemented; however, less than six months after the blackout, Red Eléctrica issued an alert emphasizing the growing urgency of ensuring voltage stability in modern power systems [16]. As the operator warned, increasing voltage interactions driven by the rapid integration of power-electronic-based generation, active market participation, and the expansion of distributed self-consumption are giving rise to complex and rapidly evolving voltage dynamics.

This event serves as a strong motivation for continued research on voltage stability mechanisms and control strategies. It illustrates that maintaining adequate voltage profiles remains a complex challenge, especially under high renewable penetration and variable load conditions. Developing improved analytical tools and control approaches for voltage stability is therefore essential to prevent similar large-scale disturbances in the future.

1.2 Research Gap and Contributions of the Thesis

To preserve normal operating conditions in distribution networks, network supervisors are deploying new voltage control devices throughout the network. These controllers are expected to operate autonomously due to limited monitoring capabilities of the network [17]. Therefore, network supervisors need to ensure that, while devices actuate, their interactions do not render the system unstable. This topic has already been addressed in the literature. Yet, the influence that picewiese affine (PWA) components, such as dead zones, can have on the interactions between control devices remains largely unexplored. This gap is particularly relevant, as general PWA theory indicates that the stability of the overall system cannot be guaranteed merely by ensuring the stability of each linear subsystem [18]. Addressing this limitation is therefore essential to improve the reliability and robustness of modern voltage control strategies.

This thesis addresses the problem of stability analysis of locally controlled voltage devices, when PWA control laws interact in ADNs. To do that, a PWA state-space model for DNs with voltage controllers (VCs) is proposed. This model is an expansion for PWA control laws of the linear state-space model proposed in [19], and for low voltage (LV) networks making use of the LV network models used in [20]. To analyse stability of voltage control interactions, the model can be applied to PWA stability analysis approaches, such as piecewise quadratic Lyapunov approaches or robust simulation approaches. Both approaches are detailed and applied in the thesis. Furthermore, proof is provided that Lyapunov-based approaches are unable to improve on the results of stability analysis found with small-signal stability analysis, making the robust simulation approach the preferred alternative for the PWA case.

1.3 Thesis Outline

This thesis is structured into five chapters.

Chapter 2 reviews the relevant literature, covering the evolution of voltage control strategies, state-of-the-art methods for ADNs, and stability analysis techniques. It also introduces the theoretical foundations of PWA systems and Lyapunov stability theory, the robust simulation approach, and the main regulatory requirements for voltage control.

Chapter 3 describes the proposed methodology, including the modeling of voltage controllers, the formulation of linear and PWA state-space models, and the development of Lyapunov-based and robust simulation approaches for stability assessment.

Chapter 4 presents and compares the results of different stability analysis methods through a set of case studies involving low and medium voltage networks with varying configurations and control laws.

Chapter 5 summarizes the main conclusions of the work and outlines potential directions for future research.

2

Literature Review

Contents

In this chapter a comprehensive review of the relevant literature pertaining to the concepts utilized in this thesis is conducted.

The first three sections of this chapter address key aspects of voltage control. The chapter begins with an overview of the evolution of voltage control techniques, highlighting the shift from traditional approaches to advanced inverter-based strategies used in modern DNs with high DERs penetration. The next section reviews state-of-the-art control strategies for ADNs, with a particular focus on droop-based methods. The third section examines recent methods for analyzing the stability of interactions between controllers.

Subsequent sections introduce PWA systems, outlining their main properties, followed by a discussion of Lyapunov theory and the techniques used to assess system stability. A review of the robust simulation method for studying the stability of PWA systems is then presented. Finally, the chapter concludes with an overview of regulatory requirements for generator connection and voltage control standards.

2.1 Evolution of Voltage Control

The fundamental and pioneering discoveries made by Nikola Tesla, Michael Faraday, and Thomas Edison were instrumental in facilitating the widespread daily use of electricity. Despite its contemporary ubiquity, the system for generating, transmitting, and distributing electric power is arguably one of the most complex and valuable feats of engineering ever conceived and constructed by humankind.

Given that electrical energy generation typically occurs at significant distances from points of consumption, extensive transmission and distribution networks are indispensable for conveying this power. The network's systems are tasked not only with transporting energy but, critically, with maintaining fundamental electrical parameters, such as voltage magnitudes and frequency, within precisely defined, acceptable ranges. Failure to do so, resulting in the electrical supply reaching end-users outside these specified limits, can cause damage to their equipment and jeopardize its proper functioning. Furthermore, robust voltage control is imperative to ensure the efficient transmission of power from generation to load centers.

In the early stages of power systems, voltage control was accomplished through mechanical means, involving manual interventions. Transformer-based mechanisms, such as on-load tap changers (OLTCs), played a crucial role in the context of electrical power systems voltage regulation. These devices have the capacity to regulate the turns ratio of their windings, thereby enabling the control of the voltage output without interrupting the load current [21]. Additionally, passive elements that are capable of injecting and absorbing reactive power, such as shunt capacitors and synchronous condensers, played a significant role in the regulation of the voltage magnitude in the electrical grid [22]. A significant development in this field was the development of automatic voltage regulation (AVR) connected to the generators. The purpose of these devices is to stabilize the voltage outputted by generators when subjected to variable loads.

In the middle of the 20th century this study area has undergone a major transformation with the introduction of flexible AC transmission systems (FACTS) by Dr. Narain G. Hingorani in the seminal paper [23]. Advances in power electronics and increased availability of these technologies have led to their use in controlling key electrical parameters that govern power flow and voltage. The fundamental principle of FACTS technology is based on the utilization of thyristor-based controllers, thereby conferring an unparalleled degree of command over electrical grids. In his work, Hingorani presented two main FACTS controllers capable of regulating voltage. The static VAr compensator (SVC) is a device that has been developed for the purpose of injecting reactive power into the network. This is achieved by switching ON and OFF combinations of capacitors and inductors, which are connected in parallel with the network. However, the performance of this device is surpassed by that of the static condenser (STATCOM). The STATCOM has been shown to offer superior performance in terms of delivering reactive power when compared to traditional SVC, particularly in scenarios where system voltages are low. It has been demonstrated that both of these devices possess the capability to dampen oscillations in addition to voltage control. Furthermore, the STATCOM has been shown to enhance transient stability due to its rapid injection and absorption capacity for reactive power, even in circumstances where the system voltage is depressed following a significant disturbance, such as a fault [23].

The paradigm of power systems is subject to constant evolution, undergoing significant transformations in the contemporary era. The introduction of new DER across the entire network has introduced a challenge in maintaining adequate voltage levels within acceptable limits. This is primarily due to the fact that DER, which are predominantly comprised of renewable energy technologies, exhibit intermittent behavior. This characteristic of the new DER make the dynamic of the network system faster and complicates prediction accuracy. Thus, technologies like OLTC that usually are operated in slow time scales can not handle the fast changing behavior of DER,

Furthermore, in contrast to traditional power systems where voltage typically diminishes along feeders, the proliferation of DER means this assumption no longer holds. Indeed, the active power injected by these dispersed units can cause a voltage increase along the feeder. In today's context, this voltage rise is mitigated by means of passive strategies such as network reinforcement. Nevertheless, this approach constitutes a highly cost-ineffective method of resolving the voltage rise issue [24]. Henceforth, novel active strategies will be formulated and disseminated across the DN, leveraging the capabilities of inverter-based generators, in order to enhance the efficiency of problem resolution.

2.2 Voltage Control Strategies

The proliferation of new technologies across the electrical network has given rise to opportunities for the development of novel control methods, which are currently under study. In contrast to the past, a significant proportions of generators are now connected to the grid via smart inverts. These inverters possess the capability to regulate certain electrical quantities, including active or reactive power injections [25]. Additionally, the volume of data available for the electrical network is increasing at an accelerated rate. Consequently, these controllers are now capable of making decisions based on a significantly greater amount of information compared to the past.

In transmission networks, voltage regulation is primarily achieved through reactive power control, as these systems typically exhibit a high reactance-to-resistance ratio ($X \gg R$). Yet, the transmission of reactive power over long distances is impractical due to the highly inductive nature of transmission lines. Consequently, voltage regulation is mainly accomplished through the use of local equipment distributed throughout the network [26]. On the other hand, DNs, the voltage magnitude is considerably less sensitive to variations in reactive power, making active power adjustments the predominant means of control.

In an effort to enhance voltage regulation, system operators and utilities have implemented a variety of methodologies. Yet, the majority of these methodologies are limited to power factor correction, necessitating a substantial investment in increased installed capacitor banks [27]. Nevertheless, most DER that have been integrated into the network can be controlled to reduce the voltage deviation problem and achieve a more efficient network utilization. The capacity for communication between the various agents will determine the role that the DSO will assume.

In the event that the DSO is unable to communicate with the controllers or chooses not to do so, a local control scheme will be adopted. Local control schemes are not dependent on any communications, as in this approach, the controllers act only based on the measurements taken by themselves [28]. Thus, this type of strategy is the most scalable and practical solution to be implemented since DN are, in their large majority, weakly monitored, having few real-time meters compared to the number of measurable quantities [29, 30].

In the study by Baker et al. [31], a local control approach is proposed in which the active and/or reactive power output of DER is adjusted proportionally to the voltage deviation in response to local changes in voltage level. It is considered that the droop coefficients of the controllers are updated on a slow time scale (every 5-15 minutes) based on the knowledge of the network and the updated load and generator forecasts. The real-time operation is performed on a fast time scale (sub-second), and the injected active/reactive power injections are adjusted based on the previously computed droop coefficients. It is essential to emphasize that the adjusted power injection should be within the limits of the controller. In the event that it is not, it should be projected into the feasible operation set. For conventional systems, such as PV or battery technology, the authors argue that the projection operation can be computed in closed form.

In [20], an approach was proposed to approximate the response dynamics from PI-controlled local devices in LV networks with linear $P(V)$ control laws. The proposed approach was developed to prevent unstable or oscillatory behaviors from the corresponding control process by adjusting the slopes (droop values), and the dead-zone width, of the control laws. This approach was expanded in [32] to include linear $Q(V)$ control laws. In this paper it is demonstrated that attempting to regulate both active and reactive power at the local level simultaneously can lead to system instability. However, if at any given time, the controller only updates the reactive or active power, the system stability is improved. Yet, it is noteworthy that, in this manner, a line exists in the P/Q plane where each point constitutes a valid solution to the given voltage deviation. Consequently, the voltage deviation can be corrected by different combinations of active and reactive power. The following algorithm is proposed to determine a voltage deviation correction that maximizes active power. The procedure iteratively adjusts the reactive power until the apparent power limit is reached. At this point, the active power is updated, and the reactive power is subsequently readjusted, continuing until a solution that compensates the voltage deviation is obtained. Since this approach does not rely on centralized control, the existence of a power flow solution is not guaranteed, and oscillatory behavior may arise. To address this limitation, a master controller is proposed to ensure that a feasible power flow solution always exists. Furthermore, to identify all possible solutions, a graphical method based on the intersection of manifolds is employed, as conventional techniques such as the Newton–Raphson method converge to a single solution only. This work was further expanded in [19], by proposing a linear state-space model that allowed for the modeling of power-flow control laws, necessary for stability analysis of networks with soft-open-points. In [33], a deep reinforcement learning algorithm was proposed to optimize linear local $Q(V)$ control laws form as a Markov decision process algorithm. The authors argue that the proposed method ensures cooperative behavior among controllers and provides fast control performance, effectively minimizing power losses and enabling rapid responses to real-time voltage fluctuations.

In contradiction to local control schemes, distribution control relies on a limited range of communications [34]. According to [35], using just small range communications, it is possible to increase the performance of the control strategy. This paper proposes a voltage control strategy in which each node is capable of communicating with its neighboring nodes. This communication enables the nodes to utilize the received information to calculate the optimal reactive power injection, thereby addressing the voltage deviation more efficiently.

The presence of effective communication among the nodes in the DN enables the DSO to assume a central control role. A centralized optimization algorithm that adjusts the parameters of the local controllers, both for active power curtailment and reactive power injection, is proposed in [36]. It has been observed that, in grids with low X/R values, as is typically the case with DN, the voltage in one phase can be reduced with a reduced reactive power injection in another phase, as opposed to the absorption of reactive power within the specific phase itself. In this manner, the proposed central optimization of all the local control parameters can take this into account.

The authors in [37] propose a centralized control scheme based on model predictive control. The linear model is based on the sensitivity of bus voltages with respect to power injections. These injections can be obtained from the inverse of the Jacobian matrix extracted from an offline power flow calculation. The control approach has been demonstrated to possess the capacity to compensate for modeling inaccuracies and measurement noise.

2.3 Voltage Stability Analysis

In contemporary society, energy networks have become the foundational systems upon which the daily lives of humans residing in developed countries are contingent. However, it must be acknowledged that, on occasion, people are made aware that power systems are not flawless; rather, they are complex entities that are susceptible to failure. These occasional failures are most of the time caused by instabilities in the power system, which can have numerous causes and be classified in various ways. Historically, the most attention has been paid to rotor angle transient stability. However, with the proliferation of new technologies, there is now a greater possibility of the occurrence of several other stability problems in power systems [38]. In Figure 2.1, the different classifications of power systems stability are delineated. The voltage stability problem, which is the focal point of this thesis, is highlighted.

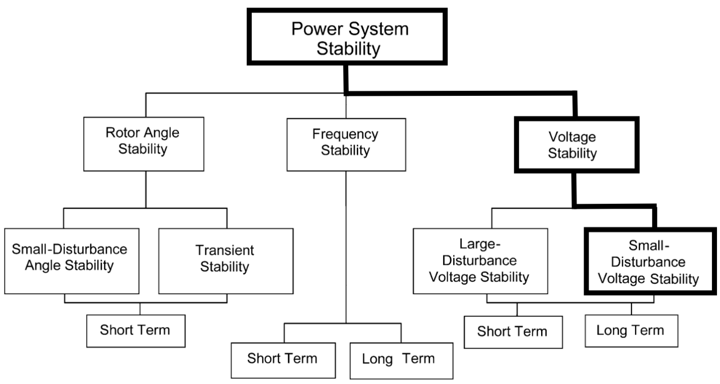

Figure 2.1: Classification of power system stability. Image adapted from [38].

The definition of power system stability proposed in [38] is as follows:

> *Power system stability is the ability of an electric power system, for a given initial operating condition, to regain a state of operating equilibrium after being subjected to a physical dis-*

turbance, with most system variables bounded so that practically the entire system remains intact.

The primary focus of this work concerns voltage stability, which is defined as the capacity of a power system to maintain uniform voltage levels across all nodes within prescribed limits following a disturbance from a designated initial operating condition. This is an emerging problem due to the proliferation of DER that change the typical voltage profile of the electrical networks. It has been observed that, several control strategies are being developed to regulate this problem. Nevertheless, these strategies modify the dynamic of the power system, thereby necessitating the assurance that the dynamic remains stable.

As demonstrated in [20], there is a significant issue with local control strategies. The demonstration begins by establishing that a modification in active power injection at a specific network node will have an impact on the voltage magnitude across all network nodes. Therefore, given that the nodes are connected to distinct phases, reducing power in one node results in a decrease in voltage at that node while increasing the voltage at nodes connected to different phases. Therefore, if the system operator employs an ON/OFF active power curtailment approach, there is a possibility that this may lead to an unstable solution. In this paper, a global control approach is proposed. This approach involves minimizing power injection, which is done subject to a droop-based equation. Yet, it is also suggested that a local control strategy can be employed. The absence of inter-node communication characterizes this solution. However, the number of iterations required to reach convergence can be excessive, and the convergence process may exhibit oscillatory and unstable characteristics.

The authors in [19] propose a linear discrete-time state-space that captures the slow interactions between multiple controllers, combining the power flow dynamics with the droop control equations. A linear state-space is proposed, in which the state variables are defined as the voltage magnitude and the voltage angle in order to be able to model power flow quantities. The system's stability can be ascertained by the condition that all the eigenvalues of the dynamic matrix lie within the unit circle. Conversely, oscillatory behavior is exhibited when at least one of the eigenvalues falls outside the unit line segment $[0, 1]$. A test network was utilized to assess the stability of the control strategy across various combinations of droop coefficients. The regions where the control was stable were identified using the eigenvalues method. Nonetheless, this approach is only capable of verifying stability for linear control laws, which is not always applicable.

The study in [39] present a decentralized voltage control method for converter-based DER that combines reactive power support and active power curtailment. To guarantee stable interactions between controllers, the system is modeled as a piecewise-linear state-space system, and stability is ensured by verifying that the eigenvalues of each linear subsystem lie within the unit circle. Yet, the control laws in this paper does not include any dead-zone

In [40], the control curves are modeled through the implementation of a discrete-time model. Yet, in this approach, the control curves are allowed to be nonlinear. It starts by demonstrating that a unique equilibrium point for the reactive power injections exists if the Volt/VAr droop curves are continuous and weakly decreasing. The authors demonstrate that a low-pass filter coefficient that ensures stability between control laws for radial networks can always be found. Yet, this coefficient is computed based solely on the maximum slope from the available control laws, without explicitly considering other piecewise components, such as dead-zones. This paper is expanded in [41], by making the stability analysis no longer limited by the radial topology of the network.

Employing a game-theoretical approach, the authors of [42] propose reactive power compensation strategies by establishing stability of local Volt/VAr controllers. In this paper, although the authors consider general control functions that are non-increasing and have a bounded derivative, the stability assessment is only evaluated based on the slope of the control law.

2.4 Piecewise Affine Systems

In the contemporary era, the complexity of systems has increased considerably. As a result, it has become evident that most systems cannot be modeled simply using linear or non-linear systems. This is due to the fact that they may possess different operating dynamics, which are influenced by internal or external state-space variables. This type of systems that combine continuous dynamics with discrete events are called hybrid systems and have been the subject of much attention over the last few years [43].

In the event that the dynamic is defined by the regions of the state-space in which the system operates, the system is designated as a switched state-dependent system.

PWA systems are a specific type of switched state-dependent systems where the state-space partitions are polyhedral and the dynamics of each partition is linear.

A trajectory of a PWA systems is defined as the sequence of state-space vectors $\boldsymbol{x}_k$ satisfying the difference equation (2.1).

$$\boldsymbol{x}_{k+1} = \boldsymbol{\Phi}_l \boldsymbol{x}_k + \boldsymbol{\phi}_l, \quad \text{for } \boldsymbol{x}(k) \in R_l, \quad l \in \mathcal{L} \tag{2.1}$$

where $\boldsymbol{\Phi}_l$ and ϕ_l are the linear dynamics and affine term of each polyhedral partition of the state-space respectively, and $\mathcal{L}$ denotes the set of indexes of the polyhedron partitions.

It is important to note that this definition is not well-posed as the state-updated is twice or more times defined across the region boundaries. This problem is resolved in [44] by defining the polyhedral regions using a combination of strict inequalities as $f(x) > a$, and equations as $f(x) = a$. This means the boundaries themselves are treated as distinct, lower-dimensional polyhedral within the partition, each with its own well-defined affine map.

For the sake of convenience, the following notation for the augmented state-space will be employed throughout this thesis:

$$\bar{\boldsymbol{x}}^{k+1} = \bar{\boldsymbol{\Phi}}_l \bar{\boldsymbol{x}}^k, \quad \text{for } \boldsymbol{x} \in R_l, \quad l \in \mathcal{L} \tag{2.2}$$

$$\bar{\boldsymbol{\Phi}}_l = \begin{bmatrix} \boldsymbol{\Phi}_l & \boldsymbol{\phi}_i \\ \mathbf{0} & \mathbf{1} \end{bmatrix}, \quad \bar{\boldsymbol{x}} = \begin{bmatrix} \boldsymbol{x} \\ 1 \end{bmatrix}. \tag{2.3}$$

Note that in this thesis, a bar above a variable indicates that the variable is in its augmented form.

As previously stated, the state-space regions of the PWA system are convex polyhedrons. These regions can be represented primarily by two equivalent forms: the H- and V-formats[45].

The first is derived from the convex hull of a finite set of points in $\mathbb{R}^n$, $X = \{\boldsymbol{x}_1, \boldsymbol{x}_2, ..., \boldsymbol{x}_d\}$.

$$P = \text{conv}(X) := \left\{ \sum_{i=1}^{d} \lambda_i \boldsymbol{x}_i \mid \lambda_1, \ldots, \lambda_d \geq 0, \sum_{i=1}^{d} \lambda_i = 1 \right\}. \tag{2.4}$$

The other one is derived from the intersection of a finite number of half-spaces, which is determined by the solution of a system of linear inequalities:

$$P = P(\mathbf{A}, \boldsymbol{b}) := \left\{ \boldsymbol{x} \in \mathbb{R}^n \mid \boldsymbol{a}_i^T \boldsymbol{x} \leq b_i \text{ for } 1 \leq i \leq m \right\} \tag{2.5}$$

where m is the number of inequalities that defined the polyhedron region. The value of this number is subject to variation depending on the complexity and number of facets of the polyhedron in question. However, it is imperative to note that the value must always exceed $d+1$ in order to form a closed polyhedron.

It is noteworthy that any polyhedral region possesses the following properties:

- Projections: Let $P \subset \mathbb{R}^n$ be a polytope and let $T : \mathbb{R}^n \to \mathbb{R}^m$ be an affine map of the form $\mathbf{T}(\boldsymbol{x}) = \mathbf{M}\boldsymbol{x} + \boldsymbol{t}$. Then $\mathbf{T}(P)$ is a polytope.
- Intersections: Let $P \subset \mathbb{R}^n$ be a polytope and let $S \subset \mathbb{R}^n$ be an affine subspace (e.g., $S = \boldsymbol{x} \in \mathbb{R}^n \mid \mathbf{E}\boldsymbol{x} = \boldsymbol{f}\}$ for some $\mathbf{E}, \boldsymbol{f}$). Then $P \cap S$ is a polytope.

Therefore, it can be concluded that the utilization of these two properties on any polytope guarantees the outcome will also constitute a polytope. This is an importance result for the Robust Algorithm presented in Section 3.7.

2.5 Lyapunov Theory

In the context of system stability analysis, it is imperative to define stability and explore methodologies for demonstrating that a system with known behavior is stable.

Although asymptotic convergence, defined as the system's state ($\boldsymbol{x}$) eventual convergence to an equilibrium point ($\boldsymbol{x}^*$) following an infinite number of iterations, $\lim_{k \to \infty} \boldsymbol{x}_k = \boldsymbol{x}^*$, is a salient feature of the system, it is imperative to note that this convergence is not the sole determining factor in the system's behavior. It is also frequently desired that the system's state remain in a close region when it is slightly disturbed. This property is referred to in the literature as Lyapunov stability [46]. Therefor, a system of type $\boldsymbol{x}_{k+1} = \boldsymbol{g}(\boldsymbol{x_k})$ with an equilibrium point at $\boldsymbol{x} = \boldsymbol{0}$ is Lyapunov stable if it satisfies equation 2.6.

$$||\boldsymbol{x}_0|| < \delta \implies ||\boldsymbol{x}_k|| < \epsilon, \forall k \geq 0 \tag{2.6}$$

The definition of stability is vague, thus it is sometimes unsatisfactory from an engineer point of view[47]. In addition, a system can be called asymptotically stable if it is stable and also verifies equation (2.7). The system is termed globally asymptotically stable if $\Omega = \mathbb{R}^n$.

$$\lim_{k \to \infty} \boldsymbol{x}_k = 0, \ \forall \boldsymbol{x}_0 \in \Omega \tag{2.7}$$

Finally, if a system is stable and there exist constants $\alpha > 0$ and $\gamma \in (0, 1)$ such that equation (2.8) is verified, the system is said to be exponentially stable.

$$\|\boldsymbol{x}_0\| < \delta \implies \|\boldsymbol{x}_k\| \leq -\alpha \|\boldsymbol{x}_0\| \gamma^k, \ \forall k \geq 0. \tag{2.8}$$

The Figures 2.2 illustrate the definitions of stability and asymptotic stability.

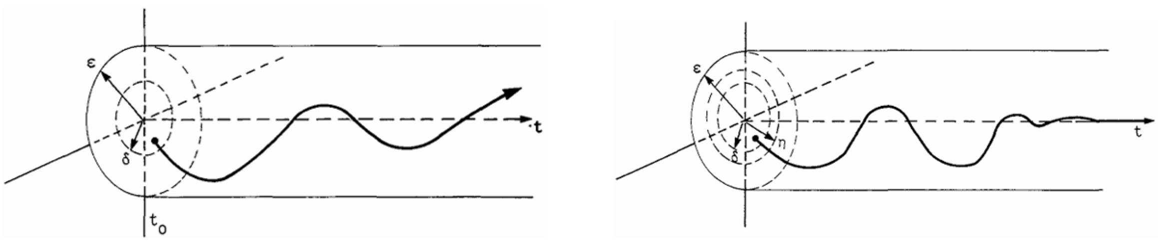

(a) Stability. **(b)** Asymptotic stability.

Figure 2.2: Stability concepts definition visualization. Figure extracted from [47].

A stable equilibrium point ensures that the system does not diverge to infinity and that the sequence of future state vectors will be contained within a radius from the equilibrium point. However, the radius may be substantial. Conversely, asymptotic stability ensures the convergence of the system state to the equilibrium point.

2.5.1 Lyapunov Function

The fundamental premise of Lyapunov's theory revolves around the concept of a Lyapunov function. This is a scalar function that can be conceptualized as a generalized measure of the "energy" of a system. The system is guaranteed to be stable if the function is shown to continuously decrease over time and is only zero at the equilibrium point. Known as the "direct method," this approach enables the assessment of stability without the explicit resolution of the system's differential or difference equations.

To be qualified as a Lyapunov function and prove stability of a system, a function has to satisfy the inequalities in (2.9). Furthermore, in the event that the function $L(\boldsymbol{x})$ is radially unbounded, i.e. $\|\boldsymbol{x}\| \to \infty \implies L(\boldsymbol{x}) \to \infty$, and $\Omega = \mathbb{R}^n$, the function is called Global Lyapunov function and the equilibrium point $\boldsymbol{x}^*$ is globally asymptotically stable [46].

$$L(\boldsymbol{x}^*) = 0 \tag{2.9a}$$

$$L(\boldsymbol{x}) > 0, \quad \forall \boldsymbol{x} \in \Omega \backslash \boldsymbol{x}^* \tag{2.9b}$$

$$L(\boldsymbol{x}_{k+1}) - L(\boldsymbol{x}_k) \leq -\alpha(\boldsymbol{x}_k), \quad \forall \boldsymbol{x} \in \Omega \backslash \boldsymbol{x}^* \tag{2.9c}$$

where $\alpha : \mathbb{R}^n \to \mathbb{R}$ is a continuous positive semi-definite function, and $\boldsymbol{x}^*$ is an equilibrium point of the system.

If such a function can be constructed over an equilibrium point of a dynamic system, then the equilibrium point is asymptotically stable in the region Ω [46].

The search for a Lyapunov function is a complex process as there is no universally applicable, one-size-fits-all approach to find a Lyapunov function for a given system. Nevertheless, in the context of linear time invariant (LTI) systems, is common to search for a quadratic Lyapunov function (QLF). This endeavor can be cast as an linear matrix inequalities (LMIs) feasibility problem, thereby facilitating the identification of the aforementioned function.

A quadratic Lyapunov function has the form of (2.10) for an equilibrium point at the origin. Since it is a quadratic function it is zero at the origin, and if $\boldsymbol{\Psi}$ is a positive definite matrix, the condition (2.9b) is also verified.

$$L(\boldsymbol{x}) = \boldsymbol{x}^T \boldsymbol{\Psi} \boldsymbol{x}, \quad \boldsymbol{\Psi} \succ 0 \tag{2.10}$$

Given the linear nature of the system, $\boldsymbol{x}_{k+1} = \boldsymbol{\Phi} \boldsymbol{x}_k$, the dynamic matrix can be utilized to formulate the condition of decreasing monotonicity along system trajectories, revealing the following:

$$
\begin{aligned}
&L(\boldsymbol{x}^{k+1}) - L(\boldsymbol{x}^{k}) < 0 \\
\equiv\ &\boldsymbol{x}_{k+1}^T \boldsymbol{\Psi} \boldsymbol{x}_{k+1} - \boldsymbol{x}_k^T \boldsymbol{\Psi} \boldsymbol{x}_k < 0 \\
\equiv\ &\boldsymbol{x}_k^T \boldsymbol{\Phi}^T \boldsymbol{\Psi} \boldsymbol{\Phi} \boldsymbol{x}_k - \boldsymbol{x}_k^T \boldsymbol{\Psi} \boldsymbol{x}_k < 0 \\
\equiv\ &\boldsymbol{x}_k^T (\boldsymbol{\Phi}^T \boldsymbol{\Psi} \boldsymbol{\Phi} - \boldsymbol{\Psi}) \boldsymbol{x}_k < 0 \\
\implies\ &\boldsymbol{\Phi}^T \boldsymbol{\Psi} \boldsymbol{\Phi} - \boldsymbol{\Psi} \prec 0
\end{aligned}
$$

In this manner, when searching for a QLF the Lyapunov conditions (2.9) became the following:

$$\boldsymbol{\Psi} \succ 0 \tag{2.11a}$$

$$\boldsymbol{\Phi}^T \boldsymbol{\Psi} \boldsymbol{\Phi} - \boldsymbol{\Psi} \prec 0 \tag{2.11b}$$

Conditions (2.10) and (2.11) are LMIs expressed in $\boldsymbol{\Psi}$. This matrix, $\boldsymbol{\Psi}$, is a symmetric matrix whose entries are variables of the LMI problem of finding a QLF. These LMI can be cast as a convex optimization problem, thus enabling the application of sophisticated and efficacious algorithms from the field of convex optimization to identify solutions [48]. If the problem of finding the entries of the matrix $\boldsymbol{\Psi}$ such that conditions (2.11) are verified, is feasible, the origin is an asymptotical stable equilibrium point. Yet, if the problem is unfeasible, nothing can be said about the stability of the system as the conditions of equation (2.11) are only sufficient.

2.5.2 Lyapunov Function for Piecewise Affine Systems

As has been established, PWA systems are systems for which the state-space is divided into a finite number of polyhedrons, with different linear dynamics applied to each region. Therefore, rather than utilizing a single dynamic matrix, $\boldsymbol{\Phi}$, it is necessary to employ multiple dynamic matrices, $\boldsymbol{\Phi}_l$, where l indexes the set of state-space polyhedrons.

2.5.2.A Common Quadratic Lyapunov Function

In accordance with the previously referenced approach, one could seek to identify a common quadratic Lyapunov function (CQLF) that would satisfy the Lyapunov conditions for every region of the state-space.

$$\boldsymbol{\Psi} \succ 0 \tag{2.12a}$$

$$\boldsymbol{\Phi}_l^T \boldsymbol{\Psi} \boldsymbol{\Phi}_l - \boldsymbol{\Phi}_l \prec 0 \quad \forall l \in \mathcal{L} \tag{2.12b}$$

Despite the numerous attempts to identify an algebraic condition for the existence of a CQLF, this endeavor has been met with success solely in the context of switching systems that have only two modes. In the context of a switching system comprising more than two modes, the existence of a CQLF shared by every combination of two nodes is a necessary but not sufficient condition for the said switching system to possess a CQLF [18].

2.5.2.B Piecewise Quadratic Lyapunov Function

Given the state-space partition on multiple polyhedrons, each with a different linear dynamic, it is reasonable to consider the construction of a Lyapunov function that is quadratic in each region. This approach suggests that each region possesses its own specific quadratic function.

Thus, instead of having a single matrix $\boldsymbol{\Psi}$ that satisfies the Lyapunov condition for every cell, m matrices $\boldsymbol{\Psi}$ can be found such that, if $\boldsymbol{x}_k \in R_i$ and $\boldsymbol{x}_{k-1} \in R_j$ the following LMIs are satisfied:

$$\boldsymbol{\Psi}_l \succ 0, \quad \forall l \in \mathcal{L} \tag{2.13a}$$

$$\boldsymbol{\Psi}_j^T \boldsymbol{\Phi}_l \boldsymbol{\Psi}_j - \boldsymbol{\Psi}_j \prec 0 \quad \forall l, j \in \mathcal{L} \times \mathcal{L} \tag{2.13b}$$

In this manner, the number of constraints increases marginally, while the number of variables also increased, thereby facilitating the resolution of the problem in terms of feasibility.

The continuity of the piecewise quadratic Lyapunov function (PWQLF) could be guaranteed using continuity matrix as presented in the work of Johansson [49]. However, as opposed to the continuous-time Lyapunov function, in discrete-time the continuity of the Lyapunov function is not required, thus this function can be discontinuous across cell boundaries, for a finite number of cells [50].

In the context of discrete-time systems, where discontinuous functions are under consideration, the system has the ability to transition between any polyhedron partition in one iteration. Therefore it is imperative to examine the condition (2.13b) for each possible region combination.

2.5.2.C Piecewise Quadratic Lyapunov Function with S-procedure

Although PWQLF considers the state-space to be divided into multiple polyhedron partitions, it does not take into account any information regarding the geometry of these partitions. Yet, in order to relax the optimization problem this information should be consider as each inequality of (2.13) only has to be verified inside a specific region of the state-space.

The S-procedure is a mathematical tool that provides a tractable way to handle quadratic conditions inside ellipsoid regions. Directly verifying such conditions is generally nonconvex and computationally intractable, since it requires checking a quadratic inequality over a region defined by another inequality. The S-procedure offers a sufficient relaxation that transforms the problem into a LMI condition, which is convex and can be efficiently verified using optimization tools.

The main steps of the S-procedure are presented next. Given a quadratic Lyapunov function $L(\boldsymbol{x}) = \boldsymbol{x}^T\boldsymbol{\Psi}\boldsymbol{x}$, the condition $L(\boldsymbol{x}) > 0$ inside an ellipsoid $\mathcal{E} = \{\boldsymbol{x} \mid \boldsymbol{x}^T\mathbf{S}\boldsymbol{x} \geq 0\}$, holds if and only if there is a non-negative scalar β such that:

$$\boldsymbol{\Psi} - \beta\mathbf{S} \succ 0 \tag{2.14}$$

where $\mathbf{S} \in \mathbb{R}^{n\times n}$ is a symmetric matrix defining the quadratic region $\mathcal{E}$.

For the intersection of multiple ellipsoid regions, the existence of positive scalars β_l such that:

$$\boldsymbol{\Psi} - \sum_{l=1}^{m} \beta_l\mathbf{S_l} \succ 0 \tag{2.15}$$

is a sufficient but not necessary condition for $L(\boldsymbol{x}) \geq 0$, $\forall\boldsymbol{x} \in \bigcap_{l=1}^{m}\mathcal{E}_l$. Conservativeness of stability is not necessarily due to the non-existence of a piecewise quadratic Lyapunov function, but due to the inability to find a set of $\boldsymbol{\beta}_l \geq 0$ that would result in the verification of inequality (2.15).

For the case of this thesis, the state-space regions, $R_l, l \in \mathcal{L}$ are polyhedral, and therefore can be expressed as half-planes as follows:

$$\boldsymbol{e}_a^T\boldsymbol{x} \geq 0 \quad \text{and} \quad \boldsymbol{e}_b^T\boldsymbol{x} \geq 0$$

where $\boldsymbol{e}_a \in \mathbb{R}^n$ and $\boldsymbol{e}_b \in \mathbb{R}^n$ are half-space coefficients. To delimitate each region one can concatenate these vectors as the following matrices, which can be referred to as cell identifiers:

$$\mathbf{E}_l\boldsymbol{x} \geq 0 \quad \forall\boldsymbol{x} \in \mathbb{R}_l, \forall l \in \mathcal{L} \tag{2.16}$$

To make these regions quadratic as the S-Procedure requires, one can multiply the two half-planes as follows [51]:

$$\boldsymbol{x}^T\mathbf{Q}\boldsymbol{x} \geq 0$$

where

$$\mathbf{Q} = \boldsymbol{e}_a \boldsymbol{e}_b^T + \boldsymbol{e}_b \boldsymbol{e}_a^T. \tag{2.17}$$

Thus, if e_{ik} denotes the kth row of $\mathbf{E}_i$, the use of the S-procedure in our case, described as the following equation, is a special case of (2.15).

$$\boldsymbol{\Psi} - \mathbf{E}_i^T \mathbf{B}_i \mathbf{E}_i = \boldsymbol{\Psi} - \sum_{j,k} \beta_{jk} \boldsymbol{e}_{ij} \boldsymbol{e}_{ik}^T, \quad \forall l \in \mathcal{L} \tag{2.18}$$

While the S-procedure is a necessary and sufficient condition for the positivity of a quadratic function on a quadratic set, it is only sufficient for verifying positivity on the intersection of several quadratic sets, which is the case in this study. Consequently, there may be a scenario in which a piecewise quadratic Lyapunov function exists yet is not found using the S-procedure.

Applying the S-procedure to the LMIs in (2.13) results in the following LMIs [52]:

$$\boldsymbol{\Psi}_i - \mathbf{E}_i^T \mathbf{U}_i \mathbf{E}_i \succ 0, \quad i \in \mathcal{L}_0 \tag{2.19a}$$

$$\bar{\boldsymbol{\Psi}}_i - \bar{\mathbf{E}}_i^T \mathbf{U}_i \bar{\mathbf{E}}_i \succ 0, \quad i \in \mathcal{L}_1 \tag{2.19b}$$

$$\boldsymbol{\Phi}_i^T \boldsymbol{\Psi}_i \boldsymbol{\Phi}_i - \boldsymbol{\Psi}_i + \mathbf{E}_i^T \mathbf{W}_i \mathbf{E}_i \prec 0, \quad i \in \mathcal{L}_0 \tag{2.19c}$$

$$\bar{\boldsymbol{\Phi}}_i^T \bar{\boldsymbol{\Psi}}_i \bar{\boldsymbol{\Phi}}_i - \bar{\boldsymbol{\Psi}}_i + \bar{\mathbf{E}}_i^T \mathbf{W}_i \bar{\mathbf{E}}_i \prec 0, \quad i \in \mathcal{L}_1 \tag{2.19d}$$

$$\boldsymbol{\Phi}_i^T \boldsymbol{\Psi}_j \boldsymbol{\Phi}_i - \boldsymbol{\Psi}_i + \mathbf{E}_i^T \mathbf{Q}_{i,j} \mathbf{E}_i \prec 0, \quad i,j \in \mathcal{T} \cap \mathcal{L}_0 \tag{2.19e}$$

$$\bar{\boldsymbol{\Phi}}_i^T \bar{\boldsymbol{\Psi}}_j \bar{\boldsymbol{\Phi}}_i - \bar{\boldsymbol{\Psi}}_i + \bar{\mathbf{E}}_i^T \mathbf{Q}_{i,j} \bar{\mathbf{E}}_i \prec 0, \quad i,j \in \mathcal{T} \cap \mathcal{L}_1 \tag{2.19f}$$

$$\boldsymbol{\Phi}_i^T \boldsymbol{\Psi}_j \boldsymbol{\Phi}_i - \boldsymbol{\Psi}_i + \mathbf{E}_i^T \mathbf{Q}_{i,j} \mathbf{E}_i \prec 0, \quad i,j \in \mathcal{T}, i \in \mathcal{L}_1, j \in \mathcal{L}_0 \tag{2.19g}$$

$$\bar{\boldsymbol{\Phi}}_i^T \bar{\boldsymbol{\Psi}}_j \bar{\boldsymbol{\Phi}}_i - \bar{\boldsymbol{\Psi}}_i + \bar{\mathbf{E}}_i^T \mathbf{Q}_{i,j} \bar{\mathbf{E}}_i \prec 0, \quad i,j \in \mathcal{T}, i \in \mathcal{L}_0, j \in \mathcal{L}_1 \tag{2.19h}$$

where $\mathcal{L}_0$ is the set of indices of regions containing the origin, $\mathcal{L}_1$ is the set of indices of regions that do not contain the origin, $\mathcal{T}$ denotes the set of possible transitions between regions, $\mathbf{U}_i \in \mathbb{R}^{nf_i \times nf_i}$, $\mathbf{W}_i \in \mathbb{R}^{nf_i \times nf_i}$, and $\mathbf{Q}_{i,j} \in \mathbb{R}^{nf_i \times nf_i}$ have nonnegative entries, and for $i \in \mathcal{L}_0$, $\bar{\boldsymbol{\Psi}}_i = [\mathbf{I}_{nxn} \mathbf{0}_{n_1}]^T \boldsymbol{\Psi}_i [\mathbf{I}_{nxn} \mathbf{0}_{n_1}]$. In this context, nf_i denotes the number of facets comprising the polyhedron region i.

If the problem of finding $\mathbf{P}_i, \mathbf{U}_i, \mathbf{W}_i$ and $\mathbf{Q}_{i,j} \forall i,j \in \mathcal{L}$, is feasible, then the origin of the PWA system is exponentially stable. If the transition inequalities are not strictly satisfied but they hold on the equalities (the Lyapunov function keeps constant along some system trajectories) the system is just stable around the origin.

2.5.3 LaSalle's Invariance Principle

In certain situations, the primary objective is not to determine the asymptotic stability of an equilibrium point, but rather to analyze the stability of a set of states within the system's state-space. In such cases, LaSalle's Invariance Principle [53] provides a powerful analytical framework for establishing convergence towards a specific invariant set, rather than to a single equilibrium point.

In practice, it is often difficult to find a Lyapunov function whose difference is strictly negative definite throughout the region of interest. Instead, one may only be able to construct a Lyapunov function whose time difference is negative semi-definite, i.e., it does not strictly decrease along all trajectories of the system. This weaker condition prevents the direct application of standard Lyapunov methods, as it cannot ensure convergence to an equilibrium point by itself.

LaSalle's Invariance Principle addresses this limitation by identifying the set of points where the Lyapunov function remains constant and demonstrating that all system trajectories will ultimately converge to the largest invariant set contained within this region. Mathematically, this set is defined as:

$$E = \{\boldsymbol{x} \mid \Delta L(\boldsymbol{x}) = 0\}, \tag{2.20}$$

where $L(\boldsymbol{x})$ is the Lyapunov-like function and $\Delta L(\boldsymbol{x})$ denotes its difference along system trajectories. According to LaSalle's principle, every solution trajectory starting within the region where $L(\boldsymbol{x})$ is non-increasing will asymptotically approach the largest invariant subset of E. This means that while the system may not converge to a single equilibrium point, it will settle into a stable set of states in which $L(\boldsymbol{x})$ remains constant.

2.6 Robust Simulation

The Lyapunov-based approaches presented in Section 2.5 are widely used to assess the stability of PWA systems [54], yet conservativeness of the results found is a strong disadvantage already reported in the literature. Michael Kanter [55] posited that for the majority of PWA systems, the Lyapunov conditions offer no insight into the system's behavior. Therefore, he proposed an alternative simulation-based approach, asserting its superiority in providing definitive answers regarding the system's behavior. This approach is referred to as robust simulation.

In the context of nonlinear systems analysis, simulation algorithms assume a pivotal role. Nevertheless, the efficacy of these algorithms is contingent upon the initial condition that is provided. Robust simulation is a methodology that has been demonstrated to effectively address this problem by considering a set of initial conditions concurrently.

Rather than employing the PWA laws of the dynamic system to map one point to another, the robust simulation maps sets to sets. In the context of polyhedral sets, which are defined by the intersection of multiple half-spaces, the mapping of one set into another can be conceptualized as a matrix multiplication [56].

The Robust Simulation algorithm has been proposed to answer the following question:

For a given set of initial states, S_0, what are all possible final states, S_f?

If the final set, S_f, is invariant, it has been proved that all initial conditions inside S_0 converge to the interior of an invariant set. Consequently, the concept of Lyapunov stability is thereby implied.

The initial step in this algorithm is to compute the intersection of the initial set, S_0, with all regions of the state-space. Given that all regions are polyhedral, the intersection of two polyhedron is itself a polyhedron. The resulting polyhedron will be mapped into another polyhedron using the corresponding linear dynamics of each region. Considering that S_1 is the set of all polyhedral partitions originated by the first iteration mapping, and L is the number of polyhedrons in the state-space, S_1 can contain up to L^2 polyhedral sets.

In the kth iteration, the set of polyhedral sets S_k can contain up to L^{k+1} polyhedra. Although this is an improbable scenario, the computational complexity of the algorithm in question can be substantial. Therefore, it is proposed in [56] a modification of the algorithm implemented by limiting the number of regions in S_j at each time step.

After each iteration, the set of reachable states, which may comprise multiple complex polyhedra, is enclosed within a single, larger polyhedron. This simplification prevents the number of polyhedra from growing exponentially, but it also means the calculated set of reachable states may include points that are not actually reachable. The algorithm is refined by increasing the number of polyhedral sets in each region that form the large polyhedron and the number of hyperplanes used to bound each set, until a definitive answer about the system stability is obtained.

The concept of computing forward reachable sets to assess the stability of nonlinear systems has been developed for continuous-time dynamic systems in [57]. In this paper, the authors propose a reachability algorithm that abstracts the original differential equations into a linear differential inclusion for each consecutive time interval by performing a first-order Taylor expansion around a linearization point.

The linearization errors, denoted by the Lagrangian remainder, are represented in an over-approximated manner. The paper presents a formula for this remainder, the calculation of which is contingent upon the second-order partial derivatives (Hessian matrices) of the system's function.

Finally, the reachable set for the subsequent point in time is ultimately determined by the dynamics of the linearized system, in conjunction with an over-approximation of the particular solution to the linear state-space equation. This calculation is further refined by a reachable set that accounts for the uncertainty inherent in the input set.

A small, verifiable region centered on the equilibrium point is thus established. The forward sets are computed until they are enclosed by the established region around the equilibrium points. In the event that this is the case, the process may reach a state of termination. Consequently, it can be posited that all solutions will ultimately converge to the equilibrium point.

The idea of the robust simulation is also explored in [58] for the case of PWA systems. However, instead of looking for a sufficient condition for stability, the authors in this paper remove all conservativeness by finding an exact characterization of the initial set.

The set $\mathcal{X}_\infty$ is defined as the largest invariant set contained within a specific region of the state-space and a set of initial condition, $\mathcal{X}(0)$, is said to belong to the domain of stability in T steps, $D_T(0)$, if $\forall x(0) \in \mathcal{X}(0)$, $x(T) \in \mathcal{X}_\infty$.

On the other hand, the set denoted by $\mathcal{X}_{inst}$ is defined as the set of states for which the system can be considered to be in a state of instability. To illustrate, in the context of state variables representing voltage magnitudes, it is imperative that these variables do not surpass a specified threshold. In the event of a threshold violation, the system should be considered unstable.

This way, the initial set is said to belong to the domain of instability $\mathcal{I}_T(0)$ if $\forall x(0) \in \mathcal{X}(0)\ \exists\, t, 0 \leq t \leq T : x(t) \in \mathcal{X}_{inst}$. It is important to note that a trajectory might reach $\mathcal{X}_{inst}$ and converge back to the origin. The term "unstable" in this paper assumes a distinct practical significance, diverging from the prevailing usage of the term in the context of traditional systems.

In essence, verifying stability in T steps entails ascertaining whether the reach set at time T belongs to the $\mathcal{X}_\infty$ set for all admissible switching sequences. However, it should be noted that this switching sequence is combinatorial with respect to T and the number of regions of the state-space. Therefore, this paper proposes a verification algorithm to circumvent such enumeration.

As the number of facets of the intersection set is subject to grow linearly with time, it is imperative that the intersection set be constrained in order to regulate the complexity of new sets. In this paper, the authors propose that the most effective approach to achieve this objective is through the utilization of hyper-rectangle approximations, in accordance with the algorithm outlined in [59] by the same author.

The verification algorithm is represented in a graph where the nodes represent sets from which a reach set evolution is computed and the weighted directed edges represent the time-steps needed for the transition. The graph is initialized with the intersection sets of the initial set with the different regions and the final $\mathcal{X}_\infty$ and $\mathcal{X}_{inst}$ sets. In the event that a set intercepts another region, a new node is inserted in the graph with the hyper-rectangle approximation.

This graph-based approach permits the execution of the graph in reverse, thereby facilitating the identification of all feasible switching sequences. Consequently, this approach enables the identification of all initial sets that converged to the unstable regions of the state-space, as well as those that converged to the stable regions.

2.7 Connection Requirements and Grid Codes

The reliable operation of a power system is contingent upon effective collaboration between the entities responsible for power generation and system operation. This is particularly crucial during periods of irregular operating conditions, where the system's stability is contingent upon the manner in which power-generating modules respond to deviations from the standard 1 p.u. voltage. From a system engineering perspective, the networks and power-generating modules are interdependent and should be treated as a unified entity to ensure system security. Given this interdependence, and because generators play a critical role in the DNs, there must therefore be requirements for connecting generators to the grid to guarantee the necessary resilience of the electricity system.

Commission Regulation (EU) 2016/631 of 14 April 2016 [60] establishes a network code defining the requirements for the connection of electricity generators to the grid, Requirements for Generators (RfG), the aim of which is to establish harmonized rules on the connection of generators to the grid to facilitate trade in electricity in the European Union, ensure the security of networks, facilitate the integration of renewable electricity sources, increase competition and enable more efficient use of the grid and resources.

Regulations applied to connecting the generators to electrical networks depend on their size, voltage levels, and effect on the overall system. If a facility has multiple synchronous machine units, each should be assessed on its size and not on its whole capacity. Yet non-synchronously connected power-generating units having a single connection point should be evaluated on their aggregated capacity [60].

Synchronous areas	**Limit for maximum capacity threshold from which a power-generating module is of type B**	**Limit for maximum capacity threshold from which a power-generating module is of type C**	**Limit for maximum capacity threshold from which a power-generating module is of type D**
Continental Europe	1 MW	50 MW	75 MW
Nordic	1.5 MW	10 MW	30 MW
Baltic	0.5 MW	10 MW	15 MW

Table 2.1: Thresholds for power-generating types in different synchronous areas.

In number 2 of article 17º of RfG for the reactive power capacity for synchronous generators of type B are presented. The same requirements apply to generators of type C. The requirements for synchronous generators of type D are in number 2 of article 19º [60].

The non-synchronous generator modules must be capable of supplying reactive power when operating at maximum capacity (P_{max} - maximum active power). It is imperative that they possess the capability to deliver reactive power that falls within the constraints of the $V - Q/P_{max}$ profile shown in Figure 2.3 [61]. Inside the region of this figure, one has the freedom to draw the curves that ensure that the system operates safely and reliably.

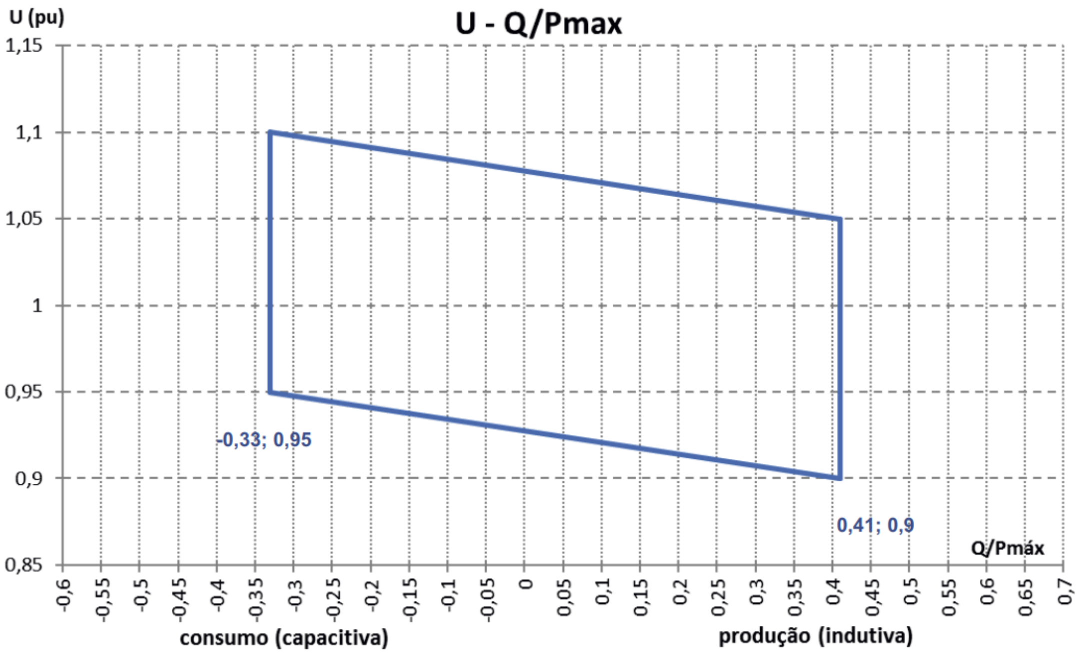

Figure 2.3: Reactive power supply capacity profile. Image extracted from [61].

The requirements for non-synchronous generators of type B are in number 2 of article 20º in [60]. The same requirements are applied to non-synchronous generators of type C and D.

In the months following the April 2025 blackout, referred in Section 1.1.3, the Spanish National Regulatory Authority revised the voltage regulation operating procedures that had been in place since 2000. The updated procedure establishes that: "Generators must have a mandatory minimum margin of reactive power capacity, both for generation and absorption, to provide the service. They must adjust their reactive power production and absorption within these limits to help maintain voltage levels at the plant bus bars within the variation margins defined by the voltage setpoint and the acceptable variation band established by the System Operator." Based on the operational curve that generators are required to follow, it is further specified that: "To assess service compliance, an acceptable deviation band of $\pm$2.5 kV around the voltage setpoint established by the System Operator for the control node is defined." This definition implies the existence of a dead-zone around the voltage setpoint, indicating that generators are expected to operate according to a PWA control curve [62].

For generators connected to very high voltage lines, Figure 2.4 illustrates the minimum reactive power support that must be provided. The service is deemed compliant when at least 75% of the sampled measurements within each hour fall within the grey area depicted in the figure.

Also, the IEEE association developed standards for the interconnection and interoperability of DER [63]. In Chapter 5 of IEEE standards document, the reactive power for power/voltage control require-

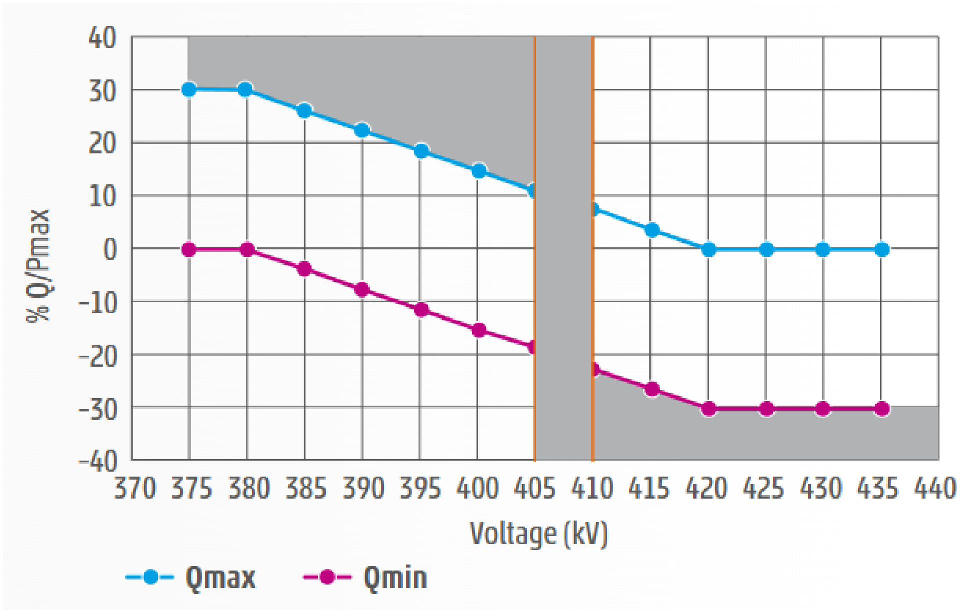

Figure 2.4: Variation of mandatory requirements for units based on the voltage of the node. Grey area in the figure below shows the right area. Image extracted from[15].

ments is stated. These requirements apply when the voltage magnitude is above 0.88 p.u. and below 1.1 p.u. The system operator of the region is in charge of defining the performance category of the DER. Yet, in annex B of [63] some guidance regarding the assignment of performance categories is provided.

DER category	Category A	Category B
Voltage regulation by reactive power control		
Constant power factor mode	Mandatory	Mandatory
Voltage—reactive power mode	Mandatory	Mandatory
Active power—reactive power mode	Not required	Mandatory
Constant reactive power mode	Mandatory	Mandatory
Voltage and active power control		
Voltage—active power (volt-watt) mode	Not required	Mandatory

Table 2.2: DER categories and their corresponding requirements.

In accordance with the specified standard, DER must possess the capability to both inject and absorb reactive power for active power outputs exceeding 5% of their rated capacity. This reactive power injection capability must be expressed as a percentage of the DER's nameplate apparent power (kVA) rating. Additionally, the DER must be capable of operating in the modes outlined in Table 2.2, with each mode being activated individually. The installed DER's default operational mode should be set to unity power factor, wherein the area system operator determines the target power factor. In this mode, the

DER is required to maintain a constant power factor within a response time of 10 seconds or less.

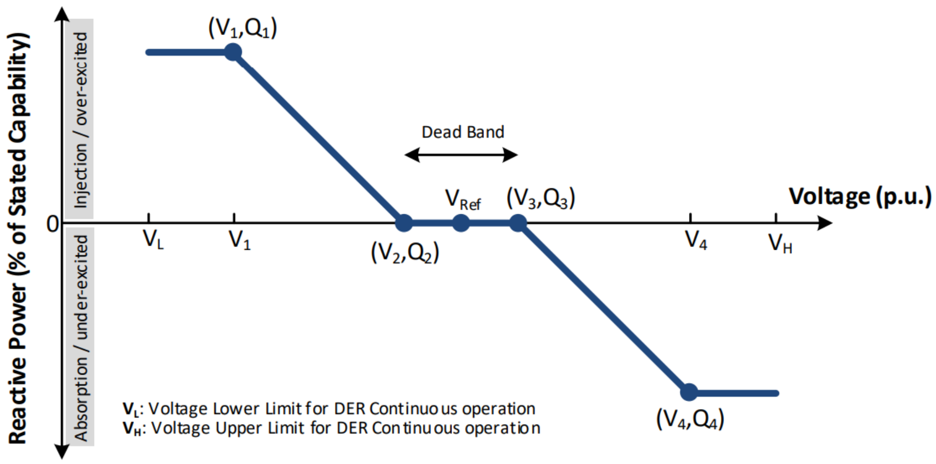

Figure 2.5: Example of voltage-reactive power characteristic curve. Image extracted from [63].

In the voltage-reactive power mode, the DER controls its reactive power output as a function of the voltage under a characteristic curve as illustrated in Figure 2.5. If not specified by the system operator the default parameters for the characteristic curve are present in Table A.1. The DER shall be capable of autonomously adjusting the reference voltage and the Volt-Var curve characteristic should change according to it.

While the IEEE 1547 standard provides default settings for smart inverters to help manage these issues, these default settings may not be the most effective for every unique electrical circuit. Thus the Electric Power Research Institute in a collaborative research project with National Grid developed an automated methodology to find the optimal, or ”tailored,” volt-var settings for the inverters [64].

The methodology for evaluating the performance of the volt-var control curves is an automated process centered on detailed simulations and a relative scoring system. For each volt-var curve under evaluation, a yearly quasi-static time-series power flow simulation is conducted, with an hourly time step. The performance of the system is evaluated by assessing the impact of each curve on eight distinct Feeder Performance Metric categories. These categories include feeder active and reactive power, power factor, system violations, equipment operations, and PV output. Subsequent to the completion of the simulations, a multi-step ranking process is initiated. Initially, the curves are ranked for each individual metric within the designated metrics categories. The summation of these individual metric scores results in the creation of a total score for each metric category. Subsequently, the curves are re-ranked at the category level. Ultimately, a weighted sum of these category rankings is calculated to produce a final score, which determines the overall best-performing curve. The objective of this process is to systematically ascertain curves that demonstrate efficacy across a range of objectives.

A case where all PV sites on the feeder, including both the National Grid site and the customer-owned sites, would utilize the selected volt-var inverter curve that was tested. Base don the metrics previous refereed the best curves are shown in Figure 2.6 and their characteristics are described in Table 2.3.

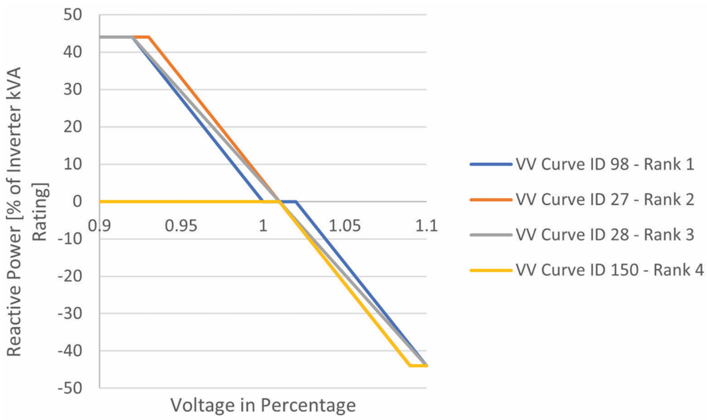

Figure 2.6: Best volt-var curves. Image extracted from [64].

Curve ID	Final Ranking	Setpoint in pu	Slope	Deadband in pu	Provide Reactive Power
98	1	1.01	5.5	0.02	Yes
27	2	1.01	5.5	0	Yes
28	3	1.01	4.88	0	Yes
150	4	1.01	5.5	-	No
IEEE1547 Cat-B	8	1.00	7.35	0.04	Yes

Table 2.3: Best volt-var curve characteristics.

An analysis of the data reveals that the four optimal performance curves exhibit comparable characteristics. The setpoint was established at a level slightly above 1 p.u., and the sloop was calibrated at approximately 5 for all four curves. A comparison of the present curve with the standard IEEE 1547 curve for category B, which achieved eighth place, suggests that the former exhibits both a substantial dead-zone and a loop that is larger than the optimal.

3

Methodology

Contents

This chapter presents the methodologies developed and applied throughout this thesis. First, the model of the voltage controllers used in the study is introduced. Then, a linear state-space model is formulated to represent the interactions among multiple voltage controllers distributed across the network. To capture the behavior of voltage controllers operating with PWA control curves, a PWA state-space model is subsequently proposed.

Following the modeling stage, the methods used for the stability analysis of PWA systems are described. The Lyapunov-based approach is first adapted to the specific problem under study, and the tools employed to solve the resulting LMI are introduced. Finally, the robust simulation algorithm is presented, along with the approximations implemented to reduce the computational complexity of the analysis.

3.1 Voltage Controller Model

Most control devices in active distribution networks are adaptations of FACTS devices from the transmission level for lower voltages. These devices are power electronics-based and use the voltage source converter as the main building block [65]. Voltage controllers are power electronic devices that provide reactive power support and adjust active power when connected to a DER. Figure 3.1(a) presents a high-level schematic of a VC connected to node i. Figure 3.1(b) illustrates the P–Q capability curve of a VC connected to a DER, where P_{max} denotes the maximum active power that the device can inject at a given moment. Similarly, Q_{max} and Q_{min} represent the maximum and minimum reactive power that the device can inject into or absorb from the grid. These limits are determined by the device's maximum apparent power and its current active power operating point.

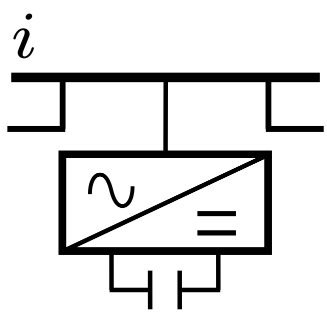

(a)

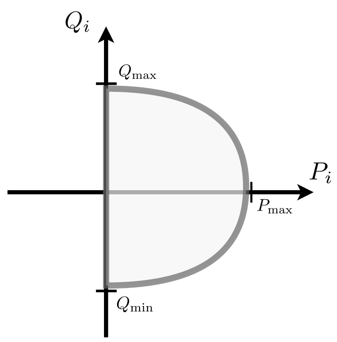

(b)

Figure 3.1: a) Voltage controller high level schematic, b) $P - Q$ capability curve of a VC connected do DER.

The operation of these devices can be described by droop-based equations as follows:

$$P^r_{k+1} - P^r_k = \delta_P \Delta m_k^{P_r} \tag{3.1a}$$
$$Q^r_{k+1} - Q^r_k = \delta_Q \Delta m_k^{Q_r} \tag{3.1b}$$

where δ_P and δ_Q are the active and reactive droops coefficients, P_r and Q_r are the active and reactive power injections at node r, and k is the discrete-time sampling instant.

These control modes can be expressed as follows:

$$\Delta m_k = \alpha^{\text{obj}} - \alpha(|\boldsymbol{V}|_k) \tag{3.2}$$

where α^{obj} is the control mode setpoint, and α can be any network quantity that can be written or approximated as a linear function of the node voltages. Defining voltage magnitude as the state variables, the quantities of α must be described in function of those. Thus, the following linear model is used [66].

$$P_{ij}(x) \approx |V_i|g_{ij} - |V_j|g_{ij} \tag{3.3a}$$
$$Q_{ij}(x) \approx -|V_i|b_{ij} + |V_j|b_{ij} \tag{3.3b}$$
$$P_i(x) \approx \sum_{j=1}^{n} G_{ij}|V_j| \tag{3.3c}$$
$$Q_i(x) \approx -\sum_{j=1}^{n} B_{ij}|V_j| \tag{3.3d}$$
$$|I_{ij}(x)| \approx \sqrt{g_{ij}^2 + b_{ij}^2}|V_i| - \sqrt{(g_{ij}^2 + b_{ij}^2)}|V_j|. \tag{3.3e}$$

where quantities g_{ij} and b_{ij} are the conductance and susceptance of the network branch. And G_{ij} and B_{ij} are the entry i, j of the real and imaginary parts of the admittance matrix.

3.2 Sate Space model

Given the integration of multiple active actors into the distribution network, it is imperative to consider their interactions. One method for representing the interactions of these actors is to construct a model of each device's behavior using functional models and equations, which are then combined into a linear state-space framework. The dynamics of a discrete-time linear system [19, 67] can be expressed as follows:

$$\boldsymbol{x}^{k+1} = \boldsymbol{\Phi}\boldsymbol{x}^k + \boldsymbol{\Gamma}\boldsymbol{u}^k \tag{3.4}$$

Neglecting the intrinsic dynamics of loads and generators that is typically very fast compared to the supervisory response, $\mathbf{\Phi}$ may be approximated by the identified matrix ($\mathbf{I} \in \mathbb{R}^{n\times n}$). Additionally, the autonomous systems control input ($\boldsymbol{u}_1$) and the input of the supervisory ($\boldsymbol{u}_2$) can be separated. The autonomous control system can be modeled as state-dependent with negative feedback, $\boldsymbol{u}_1 = -\mathbf{F}\boldsymbol{x}$. Following these assumptions, the dynamic of the state-space became described by the next equation.

$$\boldsymbol{x}^{k+1} = (\mathbf{I} - \mathbf{\Gamma}_1\mathbf{F})\boldsymbol{x}^k + \mathbf{\Gamma}_2\boldsymbol{u}_2^k \tag{3.5}$$

Based on the droop equations, the variation of active and reactive power can be expressed on the droop coefficients as follows:

$$\mathbf{\Delta P}^k = \left[\mathbf{I}_2 \odot \boldsymbol{\delta}_P\mathbf{1}^T\right]\Delta\mathbf{m}_p^k \tag{3.6a}$$

$$\mathbf{\Delta Q}^k = \left[\mathbf{I}_2 \odot \boldsymbol{\delta}_Q\mathbf{1}^T\right]\Delta\mathbf{m}_Q^k \tag{3.6b}$$

where $\boldsymbol{\delta}_P \in \mathbb{R}^n$ and $\boldsymbol{\delta}_Q \in \mathbb{R}^n$ are vectors with the active and reactive power droop coefficients. Considering n as the number of network nodes extracting the slack node, and m as the number of setpoints. The $\odot$ operator refers to the Hadamard product.

Using the linear expressions seen before, α can be expressed as a function of the state variables using the coefficient matrix $\mathbf{A}_p \in \mathbb{R}^{n\times n}$ for active power and $\mathbf{A}_q \in \mathbb{R}^{n\times n}$ for reactive power. On the other hand the objective set points ($\boldsymbol{\alpha}_{obj}$) can be incorporated in the inputs vector $\boldsymbol{u}_2$ with a coefficient matrix $\mathbf{B}_p \in \mathbb{R}^{n\times m}$ and $\mathbf{B}_q \in \mathbb{R}^{n\times m}$ for active and reactive power respectively.

$$\Delta\mathbf{m}_p^k = \mathbf{B}_p\mathbf{u}_2 - \mathbf{A}_p\mathbf{x}^k \tag{3.7a}$$

$$\Delta\mathbf{m}_Q^k = \mathbf{B}_Q\mathbf{u}_2 - \mathbf{A}_Q\mathbf{x}^k \tag{3.7b}$$

To find a linear state-space model one could take equations 3.6 and find a linear relation between the changes in magnitude ($\mathbf{\Delta}|\boldsymbol{V}|$) and argument ($\mathbf{\Delta}\boldsymbol{\theta}$), and the changes in the active ($\mathbf{\Delta}\boldsymbol{P}$) and reactive ($\mathbf{\Delta}\boldsymbol{Q}$) power. The relation between these variables is commonly called Jacobian, and the inverse of the Jacobian can be used to write a change in voltage magnitude and angle as a function of a change in active and reactive power as follows.

$$\begin{bmatrix} \mathbf{\Delta}\boldsymbol{\theta} \\ \mathbf{\Delta}|\boldsymbol{V}| \end{bmatrix} = \begin{bmatrix} \mathbf{J}_{11} & \mathbf{J}_{12} \\ \mathbf{J}_{21} & \mathbf{J}_{22} \end{bmatrix} \begin{bmatrix} \mathbf{\Delta}\boldsymbol{P} \\ \mathbf{\Delta}\boldsymbol{Q} \end{bmatrix} \tag{3.8}$$

Combining (3.7) with (3.6), and finally with (3.8), results in the following matrices:

$$\mathbf{\Gamma}_1\mathbf{F} = \mathbf{J}_{21}[\mathbf{I}_2 \odot \boldsymbol{\delta}\mathbf{1}^T]\mathbf{A}_P \tag{3.9}$$

$$\mathbf{\Gamma}_2 = \mathbf{J}_{21}[\mathbf{I}_2 \odot \boldsymbol{\delta}\mathbf{1}^T]\mathbf{B}_P \tag{3.10}$$

where $\mathbf{A}_p \in \mathbb{R}^{n\times n}$ and $\mathbf{B}_p \in \mathbb{R}^{n\times m}$ matrices set the controller modes, and the $\boldsymbol{\delta}$ vectors have the value of the droop coefficients. The inverse Jacobian elements depend on the application, one possibility is for the elements to follow the extended DC power flow approximation [68, 69].

Given the assumption that the controller setpoints remain constant $\boldsymbol{u}^k = \boldsymbol{u}^{k+1}$, one could make $\boldsymbol{\phi} = \mathbf{\Gamma}\boldsymbol{u}^k$ and use the augmented state-space difference equation (2.2).

3.3 Piecewise Affine State-Space Model

The linear state-space model presented in Section 3.2 is adequate for control laws that are linear, with slopes alone. Yet, PWA control laws, with slopes, dead- and saturation-zones require a PWA state-space model. A typical PWA PI-control law is presented in Figure 3.2 and can be expressed as follows for a $P(|V|)$ control law:

$$P_i(k+1) = \begin{cases} P_i(k), & \text{if } |V_i| < V_i^{min} \\ P_i(k) + \delta_1^i(V_i^{ref} - \Delta_{DZi} - |V_i|), & \text{if } |V_i| < V_i^{ref} - \Delta_{DZi} \\ P_i(k), & \text{if } |V_i^{ref} - |V_i|| \leq \Delta_{DZi} \\ P_i(k) + \delta_2^i(V_i^{ref} + \Delta_{DZi} - |V_i|), & \text{if } |V_i| > V_i^{ref} + \Delta_{DZi} \\ P_i(k), & \text{if } |V_i| > V_i^{max} \end{cases} \tag{3.11}$$

where P_i is the active power injection in node i, V_i^{ref} is the reference voltage of the VC of node i, $|V_i|$ is the voltage magnitude at node i, and δ_1^i and δ_2^i are the droop values of the control curve before and after the dead-zone for VC at node i.

This PWA control law implies that the system exhibits distinct dynamics across different regions of the state-space. Consequently, a PWA state-space model is required to accurately represent the overall system behavior. Each partition of the state-space model can be expressed as in (3.4), with distinct dynamic and input matrices corresponding to the regions that exhibit different dynamics. Note that $\boldsymbol{A_P}$ in (3.9), $\boldsymbol{B_P}$ in (3.10), and $\boldsymbol{\delta}$ in both may differ for each state-space partition. For instance, when the system is in a state where one or more of the VC is in the dead- or saturation-zones (i.e., the active power of that controller remains constant in that iteration), the coefficients of the matrices A_p and B_p are set to 0 for that region.

The number of state-space regions depends on the number of regions for each VC in the network.

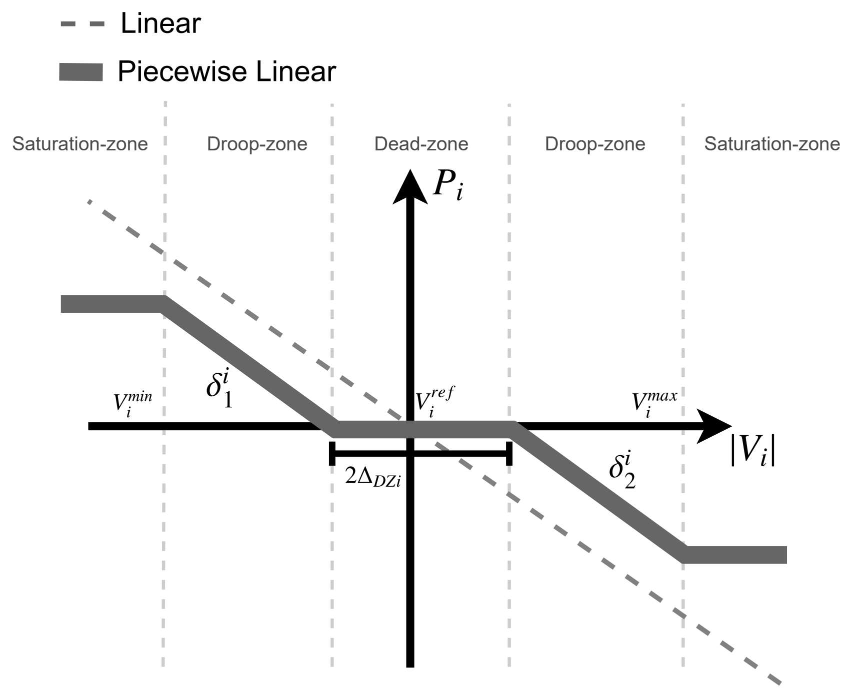

Figure 3.2: Linear and piecewise affine control curves.

This number can be expressed as follows:

$$\#R = \prod_{i=1}^{NC} \#R_i \tag{3.12}$$

where NC is the number of VC devices in the network, $\#R_i$ is the number of regions of each control law i and $\#R$ is the total number of regions of the system.

3.4 Low Voltage Network Modeling

Low-voltage networks are characterized by their proximity to end consumers, who typically consist of single-phase consumers. Consequently, the load imbalance on the difference phases is typically high. As a result, the return neutral currents can be substantial.

To model a LV network, the authors in [20] consider that the earthing system has high impedance and the system can be well represented by a four-wire circuit (3-phases and neutral) instead of a five-wire circuit. The unbalanced network voltage behavior in LV can be represented using only sensitivities to single-phase injected active power, since sensitivities to reactive power are negligible in these networks because of the high R/X ratio. This approach is used to compute sensitivities to single-phase injected power. Therefore, $\mathbf{J}_{21}$ can be substituted by the sensitivity matrix as follows:

$$\begin{bmatrix} \Delta V_1 \\ \Delta V_2 \\ \vdots \\ \Delta V_n \end{bmatrix} = \begin{bmatrix} k_{11} & k_{12} & \dots & k_{1n} \\ k_{21} & k_{22} & \dots & k_{45} \\ \vdots & \vdots & \ddots & \vdots \\ k_{n1} & k_{n2} & \dots & k_{nn} \end{bmatrix}_{|P,Q} \begin{bmatrix} \Delta P_1 \\ \Delta P_2 \\ \vdots \\ \Delta P_n \end{bmatrix} \tag{3.13}$$

To compute the sensitivity matrix, the feeder is modeled as a four-wire circuit. A power-flow is first computed for a given operating point. Then, the active power of the loads is slightly increased relative to this operating point, and a new power-flow is executed. By comparing the resulting changes in node voltage magnitudes with the corresponding changes in active power injections, the sensitivity coefficients are obtained numerically as:

$$k_{ij} = \frac{\Delta V_{ij}}{\Delta P_{ij}} \tag{3.14}$$

Using this method, the authors in [20] concluded that in the main diagonal, the sensitivities are large and positive, and outside of the main diagonal, the sensitivities are negative and smaller, meaning that local injection slightly lowers other phase voltages due to neutral coupling.

Although each node comprises three distinct phases, the state-space model adopted in this thesis only considers the phases to which loads are connected.

3.5 Lyapunov Approach

As delineated in section 2.5 the Lyapunov theory provides the conditions under which a systems is deemed asymptotically stable or stable. Given that the state-space employed in this thesis is PWA, meaning that it is divided into polyhedrons, each of which may possess a distinct affine dynamic, the most suitable and least conservative choice of function if a PWQLF. Nevertheless, conservatism in this approach may arise from two distinct origins. The choice function type, since there could exist a Lyapunov function that proves that the system is stable, but a PWQLF does't exists. Additionally, conservativeness in this approach may arise from the S-procedure, as explain in Section 2.5.2.C, since there could exist a PWQLF but it is impossible to find it with this technic of constraining the LMI to certain regions.

Under the assumption of a PWQLF it is possible to formulate the problem of analyzing the stability of the system as a set of LMI as describe in inequalities 2.19.

Some controllers may exhibit a dead-zone around the voltage reference value. Consequently, it is not reasonable to expect these devices to reach the reference value precisely. This is due to the presence of a dynamic in the dead-zone that is represented by the identity matrix. Therefore, the controllers do not modify the active and/or reactive power when their voltage magnitude is within the dead-zone. A valid criterion for ensuring the stability of interactions among multiple devices in a network is as follows: the control laws must originate a dynamic system that possesses a stable set surrounding the dead-zones of the multiple controls that have one and be near the reference value for the controllers that don't have a dead-zone

LaSalle's Invariance Principle, as seen in Section 2.5.3, states that, as time goes to infinity, the system trajectories will converge to the largest invariant set contained within the region where the derivative of the Lyapunov function is exactly zero. This way, one could search for a Lyapunov function that is non-decreasing in the dead-zone polyhedron and strictly decreasing elsewhere.

To illustrate this concept, consider a system comprised of three regions. The region with the index 2 has an identity dynamic matrix, thereby creating a dead-zone within the system. The regions R_1 and R_3 have $\bar{\boldsymbol{\Psi}}_1$ and $\bar{\boldsymbol{\Psi}}_3$ as dynamic matrices respectively. If one could find a Lyapunov function with the shape described in (3.15) it would be proven that the system will converge and stay inside R_2.

$$L(\boldsymbol{x}) = \begin{cases} \bar{\boldsymbol{x}}^T \bar{\boldsymbol{\Psi}}_1 \bar{\boldsymbol{x}}, & \text{if } \boldsymbol{x} \in R_1 \\ 0 & \text{if } x \in R_2 \\ \bar{\boldsymbol{x}}^T \bar{\boldsymbol{\Psi}}_3 \bar{\boldsymbol{x}}, & \text{if } \boldsymbol{x} \in R_3 \end{cases} \tag{3.15}$$

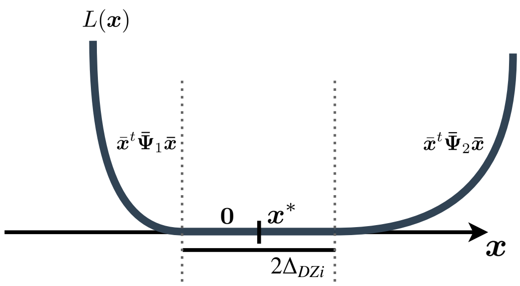

Figure 3.3: Example of a PWQLF for 1D state-space.

3.6 YAMILP

To satisfy the desired stability criteria based on Lyapunov theory, a set of LMIs must be solved. The *YALMIP* MATLAB toolbox is employed to formulate and solve these linear matrix inequalities.

Multiple solvers are available online, allowing the user to solve LMI problems, most of them free. However, these solvers take the problem descriptions differently from each other, which can be time-consuming and create difficulties for the user. *YAMILP* toolbox allows the user to model and solve their optimization problem with basically just 3 different commands. It automatically detects the type of problem the user wants to solve and selects the more suitable solver for that problem, if no solver is available it tries to converter the problem to be able to solve it [70]. The solver can also be defined manually if one wants to work with a specific solver. The following line of code can be used to create an optimization variable:

```
P = sdpvar(n, n)
```

In this case, P will be a symmetric $n \times n$ matrix. Considering that A is a matrix that has defined values one can create a list of LMI to be solved using the following line of code:

```
LMIs = [P >= 0, A'*P + P*A <= -e*eye(n)];
```

Given that semidefinite programming solvers are utilized to address convex cones, such as the semidefinite cone, which are defined as closed sets, it is imperative to consider that the formulation of the problem is constrained to include only non-strict inequalities. One might think that the solution process requires the ”hit” of a boundary to achieve convergence; therefore, these boundaries must exist. Since Lyapunov conditions are typically expressed in terms of strict inequalities, it becomes necessary to approximate non-strict inequalities with strict ones. A common and effective approach is to replace the non-strict inequality with a bound that includes a small margin, for instance by enforcing the inequality to be less than or equal to a small negative number, or greater than or equal to a small positive number.

Finally, to solve the optimization problem and retrieve the value of P one could just run the following two lines.

```
result = optimize(F);
P_solution = value(P);
```

In the problems addressed in this thesis, the value of the optimization variables are not important as it only matters if the problem is feasible or not, thus one just have to check if:

```
result.problem == 0
```

In the event that this condition is deemed to be true, the solver successfully found a solution for the set of LMI.

3.7 Robust Simulation Approach

In this thesis, a robust simulation method is employed to study the stability of PWA systems and provide a comparative analysis of the results obtained with the Lyapunov method. It is imperative to acknowledge that the conceptualization of instability in the context of this algorithm deviates from the established definition of instability within the framework of Lyapunov theory. In this case, if the forward reachable sets reach a state outside the safe limits, defined as $\mathcal{X}_{\text{safe}}$, at some iteration of the algorithm, the system is deemed unstable. Nonetheless, from a Lyapunov perspective, the system has the potential to exceed safe limits and be deemed stable, as it can theoretically converge to the equilibrium point after a finite number of iterations.

A practical approach to assess stability based on robust simulation theory enunciated at Section 2.6 is described in Algorithm 3.1.

Algorithm 3.1: Stability Analysis with Robust Simulation.

```
Input: P_0 ⊂ R^n
Output: Stability result
S ← {P_0};
while S ≠ ∅ do
    Remove P from S;
    foreach i ∈ {1, ..., m} \ {dead-zone} do
        if P ∩ R_i ≠ ∅ then
            P' ← Φ_i(P ∩ R_i);
            if P' ⊈ X_safe then
                Output: System is unstable;
                Terminate;
            else
                S ← S ∪ {P'};
Output: System is stable;
```

where $\mathcal{P}_0$ is the set of all initial states to be considered. The region defined as "dead-zone" refers to a set of states in which the power of devices is not altered by controllers.

Given a set of polyhedral regions containing all the initial states to be considered, the initial step entails the computation of the intersection between each polyhedron and each region of the state-space. For each intersection, the linear dynamics of the corresponding region are applied to the polyhedron intersection. The resultant polyhedron is then appended to the new set of polyhedrons.

During this process, when a polyhedron converges to the region where all piecewise-components are dead-zones, the polyhedron will not change state. Thus, the polyhedron can be removed from the set of polyhedron regions.

The system is considered stable after a specific number of iterations, T, if all polyhedron regions are either inside or in the neighborhood of an invariant set. On the contrary, the system is considered unstable when any polyhedron region intersects a defined limit $\mathcal{X}_{safe}$ based on normal operating limits of distribution networks.

3.8 Polyhedron Approximations

A substantial increase in the number of facets of each polyhedron can occur rapidly due to the occurrence of multiple interceptions during the forward propagation process, thereby increasing the size of the matrices describing those polyhedrons. In order to circumvent this growth, it is recommended to take an intermediate step to reduce the complexity of the polyhedron cells. One possible approach involves approximating the resultant polyhedron by an n-dimensional box that encompasses its limits. This approximation can be achieved by computing the maximum and minimum of each dimension of the polyhedron. This can be accomplished by solving a linear programming problem for each dimension of the system, maximizing and minimizing $e^T x$, where $e^T = [0...1...0]$, while ensuring that $\bar{E}\bar{x} \geq 0$. Figure 3.4(a) illustrated the outer box approximation.

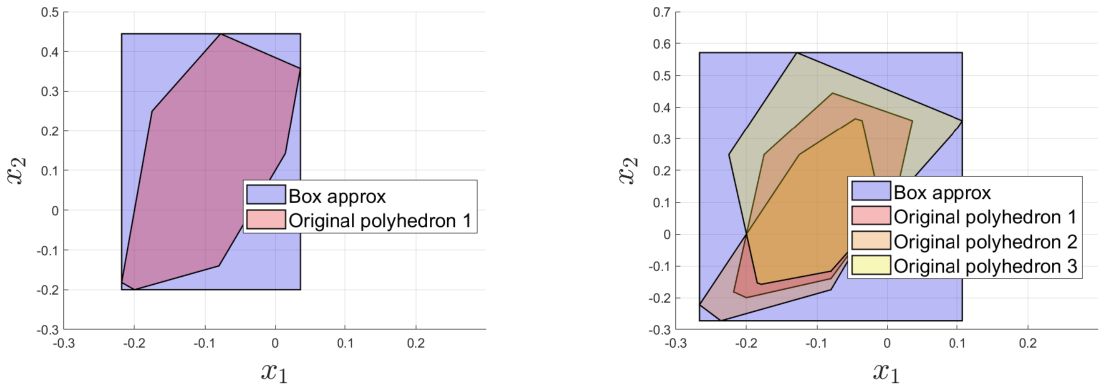

(a)

(b)

Figure 3.4: Robust simulation approximation. a) Outer box approximation. b) Merging boxes approximation.

Another source of computational complexity in the robust simulation algorithm arises from the increasing number of polyhedra, as the algorithm must perform computations for each individual cell. As illustrated in Figure 3.4(b), an additional approximation can be introduced by merging neighboring polyhedra into a single box.

This approximation mitigates the growth in the number of polyhedral cells by reducing the number of intersections and linear propagations that need to be computed.

These simplifications enable the robust simulation to be applied to more complex systems with higher-dimensional state-spaces, at the expense of increased conservativeness, since the approximation includes points that may not be reachable in practice.

4

Illustration

Contents

In this chapter, three different approaches are compared w.r.t. to their stability analysis results for PWA control laws in DN. These approaches are the following: the small-signal stability approach for the state-space model of Section 3.2, the piecewise-quadratic Lyapunov approach modeled according to the S-procedure of Section 3.5 and the robust simulation approach of Algorithm 3.1 presented in Section 3.7.

The test scenarios are defined as follows:

- **Situation I:** A two-bus LV network with 1 VC regulating the active power at its node. The control law of the VC consists of three regions: two linear slopes and one dead-zone.
- **Situation II:** A three-bus LV network with 2 VCs regulating the active power at their respective nodes. Each VC follows a control law comprising three regions: two linear slopes and one dead-zone.
- **Situation III:** A twelve-bus LV network with five VCs. Each VC regulates the active power at the corresponding node and follows a control law comprising three regions: two linear slopes and one dead-zone.

4.1 Situation I

In this situation, the two-bus LV network presented in Figure 4.1 is used. This network has a line impedance of $0.2 + j0.02$ p.u. and a VC connected to node 2, in particular to phase R. Since there is only one node in the network besides the slack node the only variable in the space state is the voltage magnitude at node 2 phase R: $\boldsymbol{x} = |V_{2R}|$ and $\bar{\boldsymbol{x}} = [|V_{2R} \mid 1]^T$.

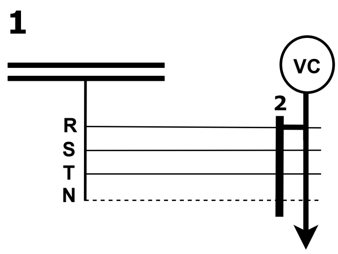

Figure 4.1: Illustration of the 2-nodes network.

According to the LV network model presented in Chapter 3 Section 3.4, the network sensitivities are as follows:

$$\Delta V_{2R} = 0.8 \Delta P_{2R} \tag{4.1}$$

The PWA control law used for the VC at node 2 can be expressed as follows:

$$P_{2R}^{k+1} - P_{2R}^{1} = \begin{cases} \delta_1(V^{ref} - \Delta_{DZ} - |V_{2R}^k|), & \text{if } |V_{2R}^k| < V^{ref} - \Delta_{DZ} \\ 0, & \text{if } V^{ref} - |V_{2R}^k| \leq \Delta_{DZ} \\ \delta_2(V^{ref} + \Delta_{DZ} - |V_{2R}^k|), & \text{if } |V_{2R}^k| > V^{ref} + \Delta_{DZ} \end{cases} \tag{4.2}$$

where $V^{ref} = 1$ p.u. and $\Delta_{DZ} = 0.02$ p.u.

In total, three regions are considered: two slopes (R_1 and R_3) and one dead-zone (R_2) located between the two slopes (for illustration purposes, the saturation-zones are not considered).

According to this control law, if the voltage magnitude $|V_{2R}|$ lies within region R_1, that is, below the reference voltage minus the dead-zone threshold, P_2 increases in order to raise the voltage magnitude. Conversely, if $|V_{2R}|$ lies within region R_3, above the reference voltage plus the dead-zone threshold, P_2 decreases to reduce the voltage magnitude. When the voltage magnitude falls within the dead-zone, no further adjustments to P_2 are made.

The corresponding piecewise state-space model can be expressed as follows:

$$x^{k+1} = \begin{cases} (1 - 0.8\delta_1)x^k + 0.8\delta_1(V_{2R}^{ref} - \Delta_{DZ2R}), & \text{if } x^k < V_{2R}^{ref} - \Delta_{DZ2R} \\ x^k, & \text{if } |V_{2R}^{ref} - x^k| \leq \Delta_{DZ2R} \\ (1 - 0.8\delta_2)x^k + 0.8\delta_2(V_{2R}^{ref} + \Delta_{DZ2R}), & \text{if } x^k > V_{2R}^{ref} + \Delta_{DZ2R} \end{cases} \tag{4.3}$$

and expressed with an augmented state as follows:

$$x^{k+1} = \begin{cases} \begin{bmatrix} 1 - 0.8\delta_1 & 0.8\delta_1(V_{2R}^{ref} - \Delta_{DZ2R}) \\ 0 & 1 \end{bmatrix} \bar{x}^k, & \text{if } x^k < V_{2R}^{ref} - \Delta_{DZ2R} \\ x^k, & \text{if } |V_{2R}^{ref} - x^k| \leq \Delta_{DZ2R} \\ \begin{bmatrix} 1 - 0.8\delta_2 & 0.8\delta_2(V_{2R}^{ref} + \Delta_{DZ2R}) \\ 0 & 1 \end{bmatrix} \bar{x}^k, & \text{if } x^k > V_{2R}^{ref} + \Delta_{DZ2R} \end{cases} \tag{4.4}$$

In the following, the stability of (4.3) is analyzed by applying the piecewise quadratic Lyapunov approach modeled according to the S-procedure of Chapter 3 Section 3.5. According to this approach, the objective is to demonstrate asymptotic convergence to a region, in this case the dead-zone. The system is deemed stable if a piecewise quadratic Lyapunov function can be found. However, if no such Lyapunov function is identified, no definitive conclusions can be drawn from the analysis, meaning that the system may be either stable or unstable.

Since the objective is to prove that the system converges to the dead-zone, the Lyapunov function can be defined as zero inside the dead-zone and piecewise quadratic for the remaining regions, as follows:

$$L(\boldsymbol{x}) = \begin{cases} \bar{\boldsymbol{x}}^T \bar{\boldsymbol{\Psi}}_1 \bar{\boldsymbol{x}}, & \text{if } \boldsymbol{x} \in R_1 \\ 0 & \text{if } x \in R_2 \\ \bar{\boldsymbol{x}}^T \bar{\boldsymbol{\Psi}}_3 \bar{\boldsymbol{x}}, & \text{if } \boldsymbol{x} \in R_3 \end{cases} \tag{4.5}$$

Consequently, it is unnecessary to verify the decrease of the Lyapunov function for transitions toward the dead-zone.

The cell-identifier matrices are built such that $\bar{\mathbf{E}}_i \bar{\boldsymbol{x}} \geq 0$ if $\boldsymbol{x} \in R_i, i \in \{1, 2, 3\}$, as follows:

$$\bar{\mathbf{E}}_1 = \begin{bmatrix} -1 & V_{ref} - \Delta_{DZ} \end{bmatrix} \tag{4.6a}$$

$$\bar{\mathbf{E}}_2 = \begin{bmatrix} 1 & -(V_{ref} - \Delta_{DZ}) \\ -1 & V_{ref} + \Delta_{DZ} \end{bmatrix} \tag{4.6b}$$

$$\bar{\mathbf{E}}_3 = \begin{bmatrix} 1 & -(V_{ref} + \Delta_{DZ}) \end{bmatrix} \tag{4.6c}$$

The application of the LMIs presented in (2.19) for the system in (4.3) results in the following LMIs:

$$\bar{\boldsymbol{\Psi}}_1 - \bar{\mathbf{E}}_1^T U_1 \bar{\mathbf{E}}_1 \succ 0 \tag{4.7a}$$

$$\bar{\boldsymbol{\Psi}}_3 - \bar{\mathbf{E}}_3^T U_3 \bar{\mathbf{E}}_3 \succ 0 \tag{4.7b}$$

$$\bar{\boldsymbol{\Phi}}_1^T \bar{\boldsymbol{\Psi}}_1 \bar{\boldsymbol{\Phi}}_1 - \bar{\boldsymbol{\Psi}}_1 + \bar{\mathbf{E}}_1^T W_1 \bar{\mathbf{E}}_1 \prec 0 \tag{4.7c}$$

$$\bar{\boldsymbol{\Phi}}_3^T \bar{\boldsymbol{\Psi}}_3 \bar{\boldsymbol{\Phi}}_3 - \bar{\boldsymbol{\Psi}}_3 + \bar{\mathbf{E}}_3^T W_3 \bar{\mathbf{E}}_3 \prec 0 \tag{4.7d}$$

$$\bar{\boldsymbol{\Phi}}_1^T \bar{\boldsymbol{\Psi}}_3 \bar{\boldsymbol{\Phi}}_1 - \bar{\boldsymbol{\Psi}}_1 + \bar{\mathbf{E}}_1^T Q_{1,3} \bar{\mathbf{E}}_1 \prec 0 \tag{4.7e}$$

$$\bar{\boldsymbol{\Phi}}_3^T \bar{\boldsymbol{\Psi}}_1 \bar{\boldsymbol{\Phi}}_3 - \bar{\boldsymbol{\Psi}}_3 + \bar{\mathbf{E}}_3^T Q_{3,1} \bar{\mathbf{E}}_3 \prec 0 \tag{4.7f}$$

In the following, the LMIs presented in (4.7) will be analysed for R_1. First, according to (4.6a), the LMI term $\bar{\mathbf{E}}_1^T U_1 \bar{\mathbf{E}}_1$ in (4.7a) can be expressed as follows:

$$\bar{\mathbf{E}}_1^T U_1 \bar{\mathbf{E}}_1 = \begin{bmatrix} U_1 & U_1(V_{ref} - \Delta_{DZ}) \\ U_1(V_{ref} - \Delta_{DZ}) & U_1(V_{ref} - \Delta_{DZ})^2 \end{bmatrix} \tag{4.8}$$

Given that the main diagonal elements of (4.8) are positive and that the determinant is zero, it can be concluded that the matrix is positive semi-definite. Therefore, for the condition (4.7a) to be satisfied, it is necessary that $\boldsymbol{\Psi}_1 \succ 0$.

The next LMI for R_1 is (4.7c). This LMI has a similar term to $\bar{\mathbf{E}}_1^T U_1 \bar{\mathbf{E}}_1$, which is $\bar{\mathbf{E}}_1^T W_1 \bar{\mathbf{E}}_1$, differing on the coefficient W_1 alone. Therefore, $\bar{\mathbf{E}}_1^T W_1 \bar{\mathbf{E}}_1$ is also a positive definite matrix and, consequently, to satisfy the LMI (4.7c), the term: $\bar{\mathbf{\Phi}}_1^T \bar{\mathbf{\Psi}}_1 \bar{\mathbf{\Phi}}_1 - \bar{\mathbf{\Psi}}_1$ must be negative definite. To be negative definite, the condition $\bar{\boldsymbol{x}}^T(\bar{\mathbf{\Phi}}_1^T \bar{\mathbf{\Psi}}_1 \bar{\mathbf{\Phi}}_1 - \bar{\mathbf{\Psi}}_1)\bar{\boldsymbol{x}} \leq 0$ needs to be verified for every $\boldsymbol{x}$.

Let $\boldsymbol{x} = \boldsymbol{v}$, where $\boldsymbol{v}$ is a eigenvector of $\bar{\mathbf{\Phi}}_1$ associated with the eigenvalue λ:

$$
\begin{aligned}
&\bar{\boldsymbol{v}}^T(\bar{\mathbf{\Phi}}_1^T \bar{\mathbf{\Psi}}_1 \bar{\mathbf{\Phi}}_1 - \bar{\mathbf{\Psi}}_1)\bar{\boldsymbol{v}} \equiv \\
&\lambda^2 \bar{\boldsymbol{v}}^T \bar{\mathbf{\Psi}}_1 \bar{\boldsymbol{v}} - \bar{\boldsymbol{v}}^T \bar{\mathbf{\Psi}}_1 \bar{\boldsymbol{v}} \equiv \\
&\quad (\lambda^2 - 1)\bar{\boldsymbol{v}}^T \bar{\mathbf{\Psi}}_1 \bar{\boldsymbol{v}} > 0 \quad \text{if } |\lambda| > 1
\end{aligned}
$$

Let $\bar{\mathbf{\Psi}}_1$ be positive definite, if $\bar{\mathbf{\Phi}}_1$ has any eigenvalue outside the unitary circle, the term: $\bar{\mathbf{\Phi}}_1^T \bar{\mathbf{\Psi}}_1 \bar{\mathbf{\Phi}}_1 - \bar{\mathbf{\Psi}}_1$ is not negative definite and, consequently, the condition (4.7c) does not hold. This result is of particular relevance, since it shows that the piecewise quadratic Lyapunov approach modeled according to the S-procedure presented in Chapter 3 Section 3.5 is unable to improve on the results of the stability analysis found with the small-signal stability for the linear state-space model of Chapter 3 Section 3.2. Similarly, the same analysis can be done for (4.7e) and for the LMIs of R_3, (4.7b), (4.7b) and (4.7b).

To validate this analysis, both the Lyapunov approach and the small-signal stability analysis for the linear state-space model [19] are compared. This comparison aims at determining the expected type of system response for a given set of droop values (δ_1 and δ_2). Combinations of droop values consider that both δ_1 and δ_2 range from 0.1 to 4 with a steps of 0.1. Note that, for the case of the linear state-space model, if any of the regions is found to be unstable, the whole system is considered unstable.

Results obtained validate the insights from the proof in (4.1), showing that the Lyapunov approach is able to evaluate stability of the system response if the eigenvalues of $\bar{\mathbf{\Phi}}_1$ lie inside the unitary circle, but is unable to provide insights onto the stability of the system response if the eigenvalues of $\bar{\mathbf{\Phi}}_1$ lie outside the unitary circle.

To assess the conservativeness of the stable regions identified through the previous approaches, simulations are performed, and the corresponding results are presented in Figure 4.2. The obtained results reveal notable discrepancies between the simulation outcomes and the stability regions predicted by the analytical methods. However, it is important to note that the simulation results depend on the chosen initial condition (in this case, $V_{2R} = 1.042$ p.u.) and the convergence criterion adopted (here defined as the difference between the last two iterations being smaller than a threshold of 10^{-6}).

To improve on the results found by simulation without considering a single initial condition, the robust simulation algorithm presented in Algorithm 3.1 can be used for a range of initial conditions, $|V_{2R}| \in [-1.1, 1.1]$p.u. The results obtained are presented in Figure 4.2 with stable regions similar to the ones found with simulation. The conservativeness found with this approach w.r.t. the stable regions from

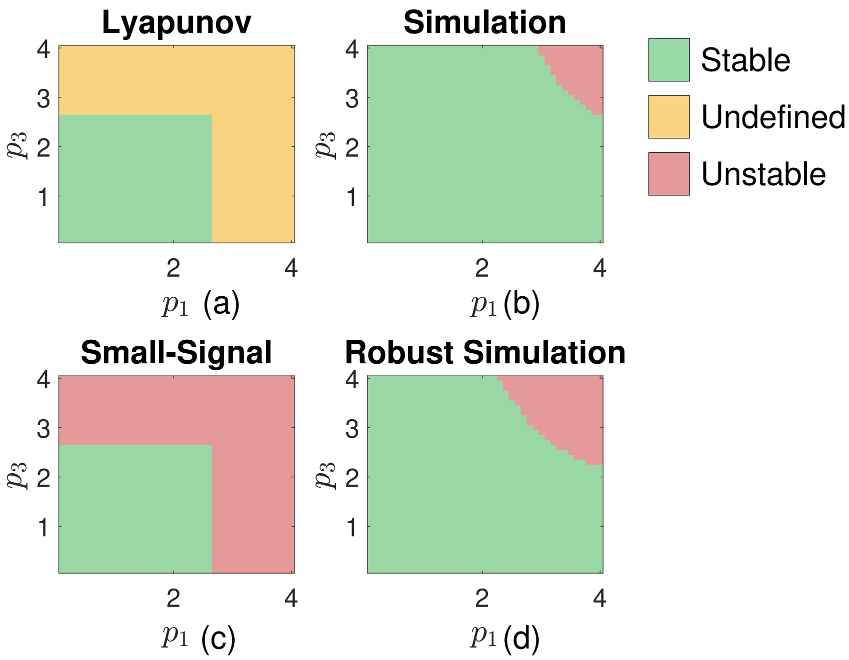

Figure 4.2: Stability regions found for the application of Lyapunov, robust simulation, small-signal and simulation approaches to the piecewise affine system of (4.3).

simulation are due to single initial condition used in simulation.

4.2 Situation II

In this situation, a three-bus LV network, presented in Figure 4.3, is used. This network has a line impedance of $0.2 + j0.02$ p.u. between the nodes 1 and 2, a line impedance of $0.2 + j0.02$ p.u. between nodes 2 and 3 and two VC connected to node 2 and 3, respectively. The VC of node 2 is connected to phase R and the VC of node 3 is connect to phase S.

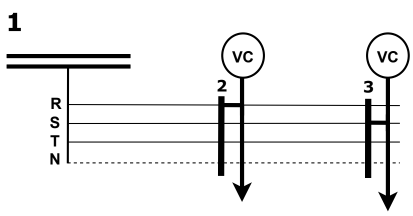

Figure 4.3: Illustration of the 3-node Network.

According to the LV network model presented in Section 3.4, the network sensitivities are as follows:

$$\begin{bmatrix} \Delta V_{2T} \\ \Delta V_{3S} \end{bmatrix} = \begin{bmatrix} 0.752 & -0.220 \\ -0.198 & 1.025 \end{bmatrix} \begin{bmatrix} \Delta P_{2T} \\ \Delta P_{3S} \end{bmatrix} \tag{4.9}$$

Assuming that outside the dead-zone and saturation zones, each VC has the same droop in the remaining control regions. The PWA control law used for both VC can be expressed as follows:

$$P_i^{k+1} - P_i^1 = \begin{cases} \delta_i(V_i^{ref} - \Delta_{DZi} - |V_i^k|), & \text{if } |V_i^k| < V_i^{ref} - \Delta_{DZi} \\ 0, & \text{if } V_i^{ref} - |V_i^k| \leq \Delta_{DZi} \\ \delta_i(V_i^{ref} + \Delta_{DZi} - |V_i^k|), & \text{if } |V_i^k| > V_i^{ref} + \Delta_{DZi} \end{cases} \tag{4.10}$$

where, i corresponds to the voltage magnitude the VC is controlling ($2R$ or $3S$). In this particular instance, the regions preceding and following the dead-zone have equal droop value for each controller. The corresponding piecewise state-space model can be expressed as follows:

$$\boldsymbol{x}^{k+1} = \begin{cases} \begin{bmatrix} 1-0.752\delta_{2R} & 0.220\delta_{3S} \\ 0.198\delta_{2R} & 1-1.025\delta_{3S} \end{bmatrix} \boldsymbol{x}^k + \begin{bmatrix} 0.752\delta_{2R} & 0.220\delta_{3S} \\ 0.198\delta_{2R} & 1.025\delta_{3S} \end{bmatrix} \begin{bmatrix} V_{2R}^{ref} - \Delta_{DZ2R} \\ V_{3S}^{ref} - \Delta_{DZ3R} \end{bmatrix}, & \text{if } \boldsymbol{x}^k \in \{R_1\} \\ \begin{bmatrix} 1 & 0.220\delta_{3S} \\ 0 & 1-1.025\delta_{3S} \end{bmatrix} \boldsymbol{x}^k + \begin{bmatrix} 0 & 0.220\delta_{3S} \\ 0 & 1.025\delta_{3S} \end{bmatrix} \begin{bmatrix} 0 \\ V_{3S}^{ref} - \Delta_{DZ3S} \end{bmatrix}, & \text{if } \boldsymbol{x}^k \in \{R_2\} \\ \begin{bmatrix} 1-0.752\delta_1 & 0.220\delta_{3S} \\ 0.198\delta_{2R} & 1-1.025\delta_{3S} \end{bmatrix} \boldsymbol{x}^k + \begin{bmatrix} 0.752\delta_{2R} & 0.220\delta_{3S} \\ 0.198\delta_{2R} & 1.025\delta_{3S} \end{bmatrix} \begin{bmatrix} V_{2R}^{ref} + \Delta_{DZ2R} \\ V_{3S}^{ref} - \Delta_{DZ3S} \end{bmatrix}, & \text{if } \boldsymbol{x}^k \in \{R_3\} \\ \begin{bmatrix} 1-0.752\delta_{2R} & 0 \\ 0.198\delta_{2R} & 1 \end{bmatrix} \boldsymbol{x}^k + \begin{bmatrix} 0.752\delta_{2R} & 0 \\ 0.198\delta_{2R} & 0 \end{bmatrix} \begin{bmatrix} V_{2R}^{ref} - \Delta_{DZ2R} \\ 0 \end{bmatrix}, & \text{if } \boldsymbol{x}^k \in \{R_4\} \\ \begin{bmatrix} 1 & 0 \\ 0 & 1 \end{bmatrix} \boldsymbol{x}^k, & \text{if } \boldsymbol{x}^k \in \{R_5\} \\ \begin{bmatrix} 1-0.752\delta_{2R} & 0 \\ 0.198\delta_{2R} & 1 \end{bmatrix} \boldsymbol{x}^k + \begin{bmatrix} 0.752\delta_{2R} & 0 \\ 0.198\delta_{2R} & 0 \end{bmatrix} \begin{bmatrix} V_{2R}^{ref} + \Delta_{DZ2R} \\ 0 \end{bmatrix}, & \text{if } \boldsymbol{x}^k \in \{R_6\} \\ \begin{bmatrix} 1-0.752\delta_{2R} & 0.220\delta_{3S} \\ 0.198\delta_{2R} & 1-1.025\delta_{3S} \end{bmatrix} \boldsymbol{x}^k + \begin{bmatrix} 0.752\delta_{2R} & 0.220\delta_{3S} \\ 0.198\delta_{2R} & 1.025\delta_{3S} \end{bmatrix} \begin{bmatrix} V_{2R}^{ref} - \Delta_{DZ2R} \\ V_{3S}^{ref} + \Delta_{DZ3S} \end{bmatrix}, & \text{if } \boldsymbol{x}^k \in \{R_7\} \\ \begin{bmatrix} 1 & 0.220\delta_{3S} \\ 0 & 1-1.025\delta_{3S} \end{bmatrix} \boldsymbol{x}^k + \begin{bmatrix} 0 & 0.220\delta_{3S} \\ 0 & 1.025\delta_{3S} \end{bmatrix} \begin{bmatrix} 0 \\ V_{3S}^{ref} + \Delta_{DZ3S} \end{bmatrix}, & \text{if } \boldsymbol{x}^k \in \{R_8\} \\ \begin{bmatrix} 1-0.752\delta_{2R} & 0.220\delta_{3S} \\ 0.198\delta_{2R} & 1-1.025\delta_{3S} \end{bmatrix} \boldsymbol{x}^k + \begin{bmatrix} 0.752\delta_{2R} & 0.220\delta_{3S} \\ 0.198\delta_{2R} & 1.025\delta_{3S} \end{bmatrix} \begin{bmatrix} V_{2R}^{ref} + \Delta_{DZ2R} \\ V_{3S}^{ref} + \Delta_{DZ3S} \end{bmatrix}, & \text{if } \boldsymbol{x}^k \in \{R_9\} \end{cases} \tag{4.11}$$

where $\boldsymbol{x}^T = [|V_{2R}|\ |V_{3S}|]$. The regions that result from the PWA state-space are presented in Figure 4.4.

For this test situation, only the robust simulation of Algorithm 3.1 was used based on the conclusions from Situation I. The propagation of reachable sets is presented in Figure 4.5 for three different parameter cases of the PWA state-space model. The light green regions represent the initial sets of each iteration, while the green regions represent the forward propagated sets of each iteration. The first initial

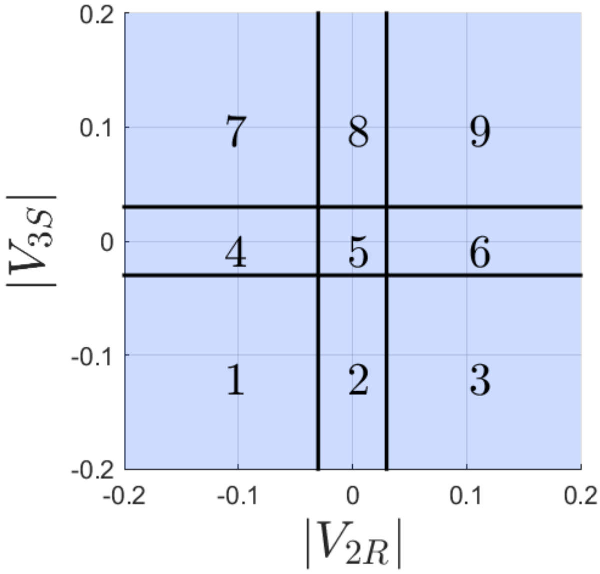

Figure 4.4: Regions of the state-space illustrative example.

region is defined as a square of size 0.2 p.u. by 0.2 p.u. centered on V^{ref}. The first case presented in Figure 4.5(a) considers: $V^{ref} = 1$ p.u., $\Delta_{DZ} = 0.02$ p.u. for both VC, $\delta_{2R} = 0.7$ and $\delta_{3S} = 0.8$. The second case, presented in Figure 4.5(b), only differs from the first case w.r.t. the droop values, increasing them to $\delta_{2R} = 2.3$ and $\delta_{3S} = 2.4$. The third case presented in Figure 4.5(c) differs from the second case w.r.t. the dead-zone, with an increase of Δ_{DZ} to 0.03 p.u.

Results obtained indicate that the system is stable for the first case, since the sets converge to region 5, which corresponds to the region where the state is in the dead-zone for both of the VC. The second case is no longer stable, since the sets do not converge to region 5. This is due to the increase of droop values. Nevertheless, in the third case it is shown that by increasing the dead-zone width it is possible to regain stability of the system response, even for greater droop values.

Stability regions are presented in Figure 4.6 for different dead-zone widths (and the same droop combinations of Situation I). Results are also validated with simulation (considering as an initial condition of $V_2 = 0.91$ p.u. and $V_3 = 0.90$ p.u.). Results obtained show that an increase in the dead-zone width increases the number of droop combinations that have a stable system response. The width of the dead-zone is, therefore, an important parameter that should be considered when analysing stability of PWA systems. Note that although these zones increase stability, the trade-off is that there is a greater deviation of the node voltages w.r.t. the reference value (even for PI control laws).

As demonstrated in section 2.7, the regulatory framework stipulates that generators must regulate the voltage magnitude within a designated parallelogram, as illustrated in Figure 2.3. Within the confines of this parallelogram, the device has the capacity to delineate a curve that is optimized to align

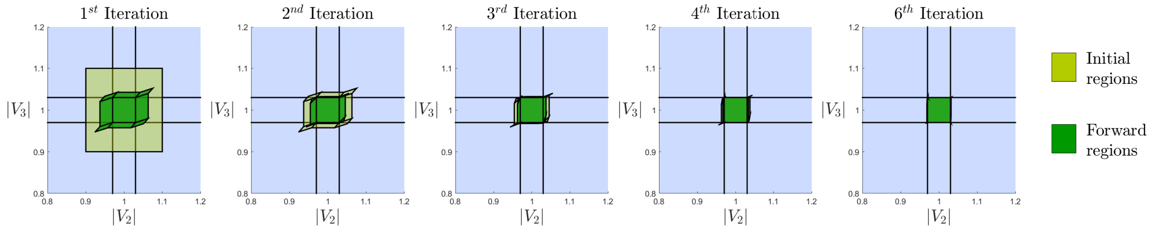

(a)

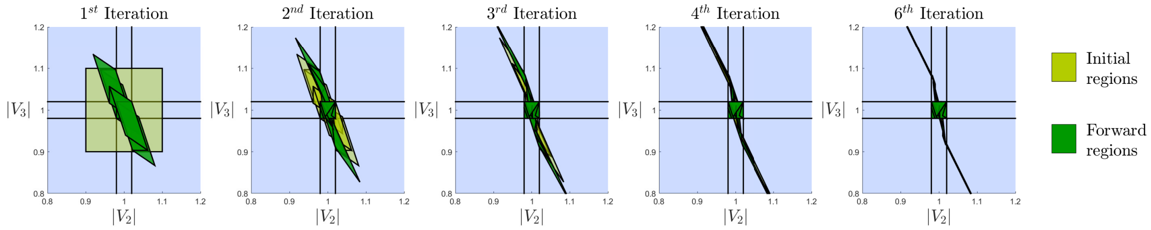

(b)

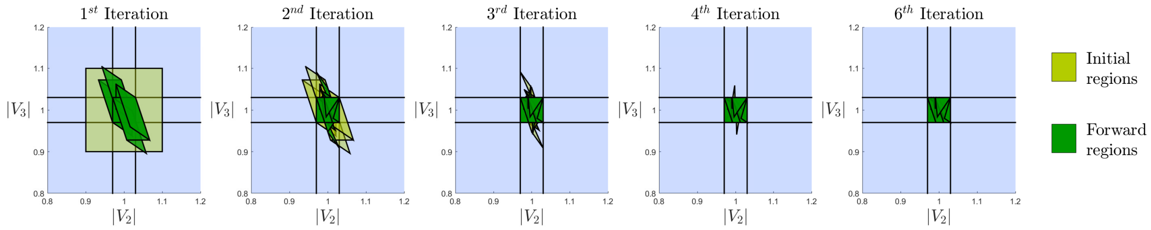

(c)

Figure 4.5: Propagation of the initial set of all voltage magnitudes between 0.9 and 1.1 p.u. for both VC of the network presented in Figure 4.3. The results obtained follow Algorithm 3.1 presented in Section 2.6 for the piecewise affine state-space model of section 3.3. The light green region in each iteration represents the initial regions, and the green regions represent the forward-propagated regions. Plots (a), (b) and (c) differ on testing parameters, specifically the droops and the dead-zone width.

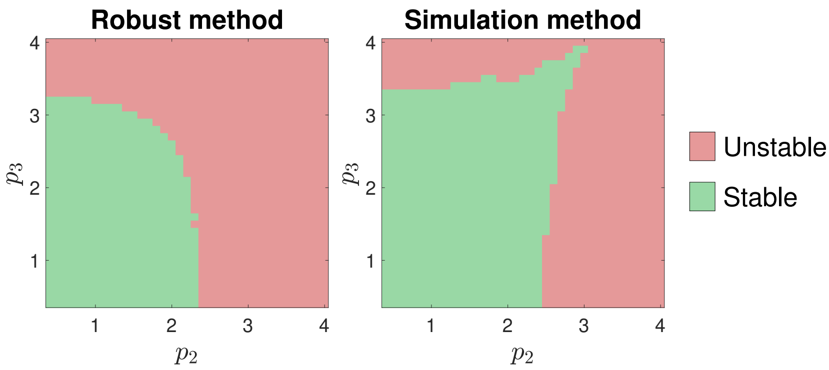

(a) Stability regions with $\Delta_{DZ} = 0.02$ p.u.

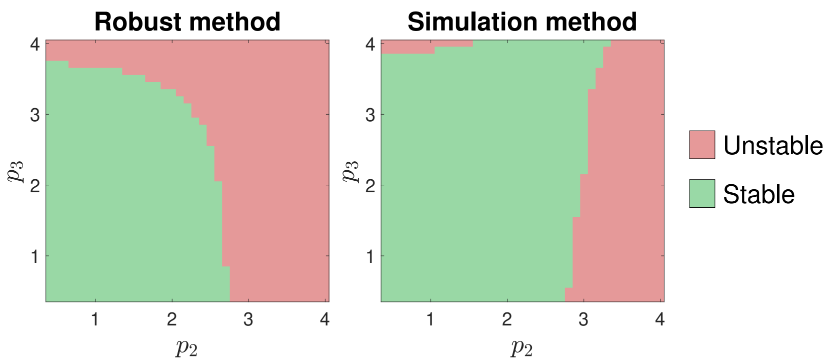

(b) Stability regions with $\Delta_{DZ} = 0.03$ p.u.

Figure 4.6: Results of the simulation and robust methods with two different dead-zones widths.

with its predetermined objectives. However, it is imperative to acknowledge the interdependence of the parameters that define the curve, particularly the dead-zone width and droops. These parameters are inextricably linked, as the curve must be meticulously tailored to conform to the specifications of the designated parallelogram. For instance, expanding the width of the dead-zone consequently increases the droops of the dynamic regions of operation.

In Figure 4.7, a set of control curves is depicted within a typical regulation parallelogram. As shown, these curves may include or exclude dead-zones and can be characterized by different droop coefficients. As demonstrated in the previous results, both parameters have a significant impact on the voltage stability of the network.

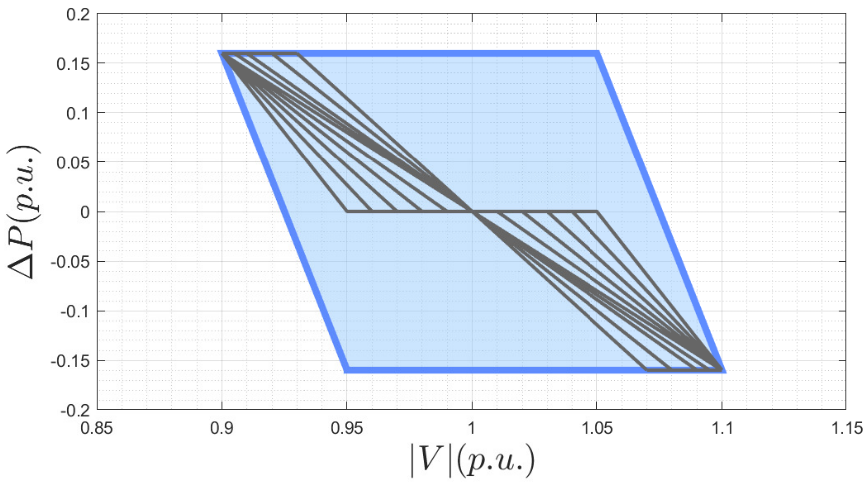

Figure 4.7: Possible control curves drawn inside a typical regulation parallelogram.

Using the network example presented in this section, and assuming that both controllers operate with identical control curves, a stability analysis was performed for multiple curve configurations employing the robust simulation method. Figure 4.8 illustrates which control curves lead to stable or unstable system behavior. The curves shown in green correspond to stable operating conditions, whereas those shown in red indicate instability. As observed, determining which control curves ensure system stability is not a straightforward task.

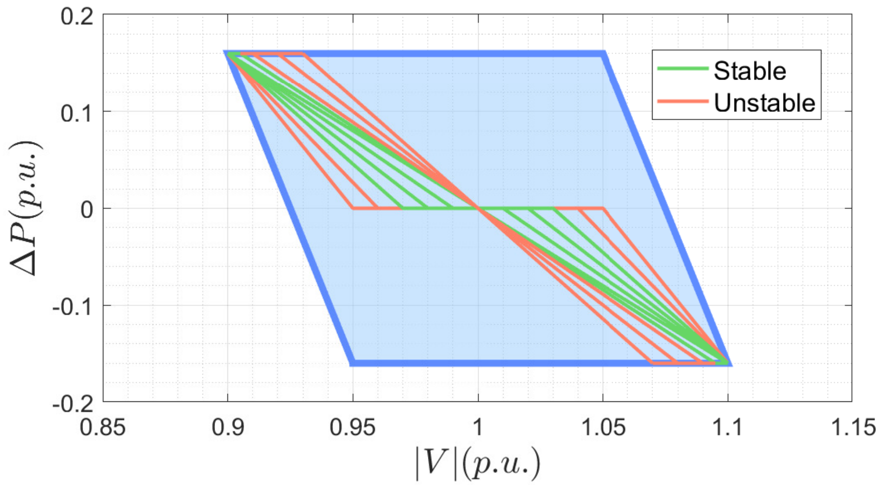

Figure 4.8: Stability analysis results of the possible curves inside a typical regulation parallelogram.

4.3 Situation III

In this test situation, a real low-voltage distribution network consisting of 12 nodes is analyzed. The network's true geographical layout is depicted in Figure 4.9. The node marked with a flag is the slack node and the state vector is defined as $x \in \mathbb{R}^{11}$, following the same approach as in previous analysis.

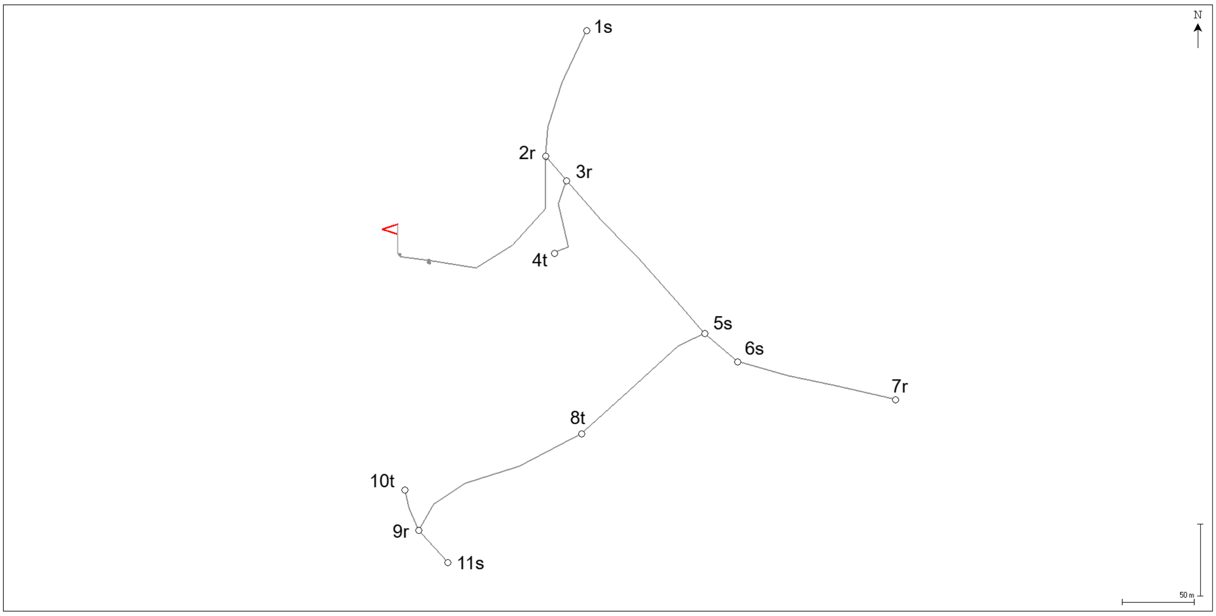

Figure 4.9: Geographic representation of a real 19-node medium voltage network.

Multiple power flow analyses were performed to determine the sensitivities of the node voltage magnitudes with respect to the injected active power at each node in the state space. The results of this sensitivity analysis are presented in (4.12).

$$
\begin{bmatrix} \delta P_{1S} \\ \delta P_{2R} \\ \delta P_{3R} \\ \delta P_{4T} \\ \delta P_{5S} \\ \delta P_{6S} \\ \delta P_{7R} \\ \delta P_{8T} \\ \delta P_{9R} \\ \delta P_{10T} \\ \delta P_{11S} \end{bmatrix} = \begin{bmatrix}
0.88 & -0.08 & -0.08 & -0.08 & 0.34 & 0.34 & -0.1 & -0.08 & -0.1 & -0.1 & 0.38 \\
-0.08 & 0.3 & 0.28 & -0.06 & -0.08 & -0.08 & 0.3 & -0.08 & 0.3 & -0.1 & -0.08 \\
-0.08 & 0.3 & 0.36 & -0.1 & -0.1 & -0.1 & 0.38 & -0.1 & 0.38 & -0.12 & -0.08 \\
-0.08 & -0.06 & -0.1 & 0.86 & -0.12 & -0.1 & -0.1 & 0.44 & -0.12 & 0.44 & -0.12 \\
0.34 & -0.08 & -0.12 & -0.1 & 1.02 & 1.02 & -0.34 & -0.24 & -0.34 & -0.26 & 1.12 \\
0.36 & -0.08 & -0.14 & -0.1 & 1.02 & 1.14 & -0.38 & -0.24 & -0.36 & -0.28 & 1.14 \\
-0.1 & 0.34 & 0.42 & -0.1 & -0.24 & -0.26 & 1.52 & -0.3 & 1.04 & -0.34 & -0.24 \\
-0.12 & -0.1 & -0.12 & 0.5 & -0.36 & -0.36 & -0.24 & 2.06 & -0.44 & 2.18 & -0.74 \\
-0.12 & -0.06 & 0.5 & -0.14 & 0.46 & -0.28 & 1.2 & -0.7 & 3.18 & -1.14 & -0.62 \\
-0.14 & -0.16 & -0.2 & 0.74 & -0.5 & -0.5 & -0.42 & 3.02 & -1.04 & 4.9 & -1.56 \\
0.52 & -0.12 & -0.12 & -0.2 & 1.54 & 1.54 & -0.46 & -0.7 & -1.3 & -1.02 & 4.34
\end{bmatrix} \begin{bmatrix} \delta V_{1S} \\ \delta V_{2R} \\ \delta V_{3R} \\ \delta V_{4T} \\ \delta V_{5S} \\ \delta V_{6S} \\ \delta V_{7R} \\ \delta V_{8T} \\ \delta V_{9R} \\ \delta V_{10T} \\ \delta V_{11S} \end{bmatrix} \tag{4.12}
$$

Nodes 1, 4, 5, 9, and 10 are considered to have a VC connected to them that is capable of controlling the active power injection of these nodes based on the control curve (4.10). This control curve has a dead-zone around the reference values and two slopes, one connecting to the right and another to the left of the dead-zone.

Since there are 5 VCs in this network, and each VC has 3 operating regions, the piecewise linear system has 243 regions. Thus in this example the robust simulation approximations will be used to reduce the computation run time of the stability analysis. In Figure 4.10 is presented the number of polyhedra and the execution time of the robust simulation algorithm, with and without approximations, during the iterative process. As shown, running the algorithm without approximations quickly becomes infeasible due to the rapid growth in the number of polyhedral regions. Without the approximations presented in Section 3.7, the algorithm could not be executed beyond three iterations because the number of polyhedral cells increased too rapidly, leading to memory limitations.

Based on the results presented in Figure 4.11 it is possible to compare iteration 3 of the robust simulation with and without approximation. This radar chart illustrates the maximum absolute deviation from

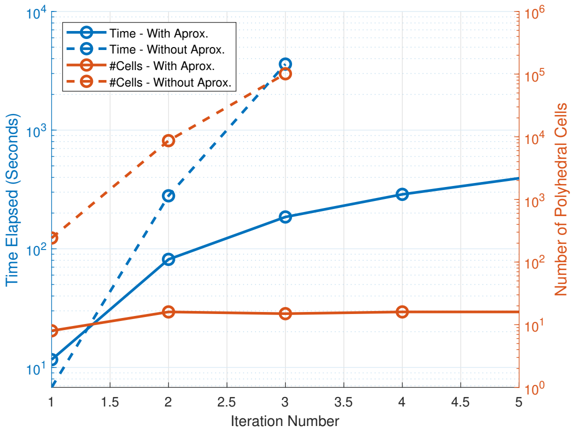

Figure 4.10: Computational complexity of the robust simulation algorithm with and without the proposed approximations.

1.0 p.u. across the union of all polyhedral reachable sets, i.e., it shows the largest deviation of the voltage magnitude at each of the 11 network nodes after three control iterations, indicating that none of the voltages exceed the values represented in the chart. As observed, the case with approximations exhibits larger deviations from the reference values, as some of the resulting points are not truly attainable due to the simplifications introduced. Yet, it is still possible to verify that the voltage magnitudes of the nodes with VCs are converging towards the dead-zone. When verifying the results of the robust simulation with approximations, one should not interpret them as the actual reachable sets, but rather as an indication of whether the system is stable or not.

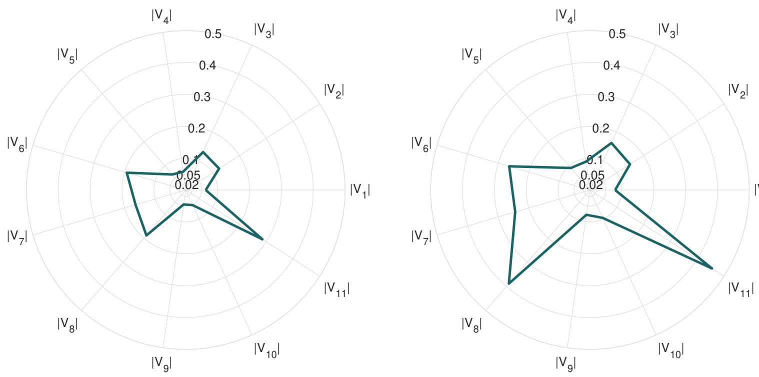

(a) Without approximations **(b)** With approximations

Figure 4.11: Maximum deviations of the forward reachable sets at iteration 3.

To assess the stability of the network under specific control laws, defined by given droop values and dead-zone widths, the robust simulation can be executed for several iterations. By observing whether the voltage magnitudes of the controlled nodes diverge or converge toward the dead-zone region, one can determine the stability of the system. Figure 4.12 presents three radar charts showing the results of the first, fifth, and tenth iterations of the robust simulation for three different control curve configurations. As before, these charts represent the maximum absolute deviation from 1.0 p.u. for the 11 nodes of the network.

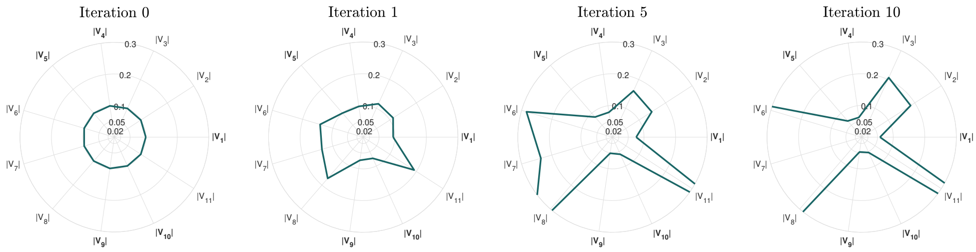

(a)

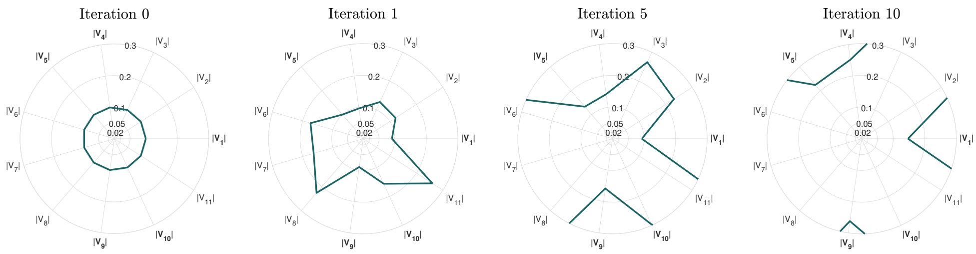

(b)

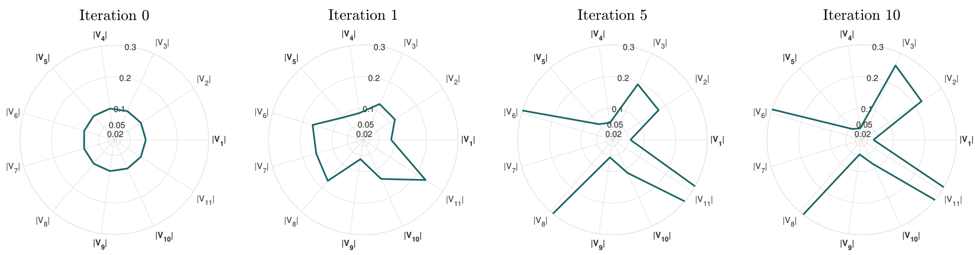

(c)

Figure 4.12: Propagation of the initial voltage magnitude set, defined between 0.9 and 1.1 p.u. (corresponding to a maximum deviation of 0.1 p.u.), for the 11 nodes of the network presented in Fig. 4.9. The results were obtained using Algorithm 3.1, applied to the PWA state-space model described in Section 3.3. Subplots (a), (b), and (c) correspond to different droop settings used in the controllers.

In the first case, presented in Figure 4.12(a), all VCs use identical parameters—setpoints of 1.0 p.u., droops of 0.2, and dead-zones of 0.02. The results show convergence: by iteration 10, all controlled nodes were clearly converging towards the dead-zone, while non-controlled nodes reach larger but bounded deviations, reflecting limited controllability rather than instability.

The second case, presented in Figure 4.12(b), employs a higher droop value of 0.35. Here, instability arises and the magnitudes of all nodes diverges from the dead-zone, with almost all voltage deviation exceeding 0.2 p.u. by iteration 10. Node 10 seems to be the one that diverges more rapidly indicating that the high droop in this node could be the main cause of instability.

Finally, the third case, presented in Figure 4.12(c), demonstrates a stabilization strategy: by reducing only the droop of node 10's VC to 0.1 (keeping others at 0..35), the system regains stability, with all controlled nodes converging to small deviations from 1.0 p.u. after five iterations.

If the system operator intends to determine which combinations of droop values and dead-zone widths lead to a stable network behavior, a parameter sweep can be performed over a range of droop coefficients and dead-zone widths. Given the large number of parameters involved, only two parameters are varied in each plot presented in Figure 4.13, the others are kept constant, allowing for a clear visualization of the corresponding stability regions.

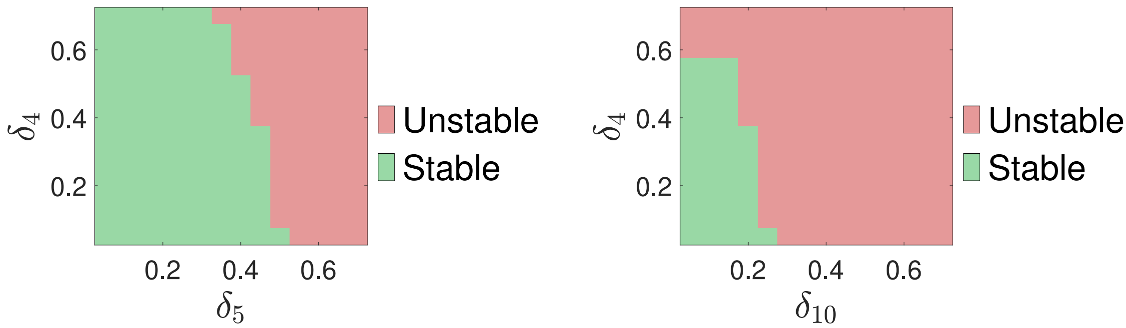

(a)

(b)

Figure 4.13: Stable regions for a droop coefficient sweep in two VCs, while keeping the others fixed at 0.1. The dead-zone width was kept constant at 0.02 for all VCs. (a) Sweep of the droop coefficients for the VCs at nodes 4 and 5. (b) Sweep of the droop coefficients for the VCs at nodes 4 and 10.

Figure 4.13(a) presents the results of the droop sweep for the VCs at nodes 4 and 5. Figure 4.13(b) shows the corresponding results for the droop sweep of the VCs at nodes 4 and 10. As observed, the droop coefficient of the VC at node 10 has a strong influence on the overall network stability, as even a slight increase in this parameter leads to unstable system behavior. When the droop value of the VC at node 10 is kept at 0.1, the droop coefficients at nodes 5 and 4 can be increased to values greater than 0.4 while still maintaining network stability.

5

Conclusion

Contents

This chapter presents an overview of the main conclusions of this thesis and outlines potential directions for future work that could provide a natural continuation of the research.

5.1 Overview

In this thesis, a PWA state-space model that captures the interactions between voltage control devices is proposed for ADN. With this model, PWA stability approaches, such as Lyapunov or robust simulation approaches, can be used to analyse stability of voltage control interactions, when control laws are PWA.

The first testing situation considered a small LV network consisting of a single node with a VC connected to it and a slack node. This simplified configuration allowed for a clear demonstration that the traditional Lyapunov-based approach commonly used for the stability analysis of PWA systems tends to be overly conservative. It was proven that, in most cases, this method yields results equivalent to performing a small-signal stability analysis. Additionally, a parameter sweep of the VCs droop coefficients was conducted, varying from 0.1 to 4 in increments of 0.1, to identify the droop values that lead to system instability.

In the second testing situation, a network with three nodes was analyzed, with two VCs connected to different phases of different nodes, and a slack node. This testing situation had the capability of illustrating the potentially harmful interactions between VCs and the risk of voltage instability. Since the network includes two nodes, each with a VC operating under a PWA control curve with a dead-zone around the reference voltage, the state-space, defined in $\mathbb{R}^2$, is divided into 9 polyhedral partitions. Based on the conclusions drawn from the first situation, only the robust simulation method was employed for this test. Assuming both VCs share identical control curves, the propagation sets for three different control configurations were obtained for the first six iterations. The results showed that increasing the droop values of the control curves causes the reachable sets to expand rapidly, leading to system instability. However, the analysis also revealed that, for the same droop values, the system can be stabilized by slightly increasing the width of the dead-zone. To ensure compliance with regulatory requirements, multiple control curves within a typical regulatory parallelogram were tested. The results showed that selecting an appropriate control curve is not straightforward when aiming to guarantee system stability, as increasing the dead-zone width simultaneously requires larger droop values to remain within the regulatory limits. The utilization of the robust simulation method facilitated the verification of the control curves that ensured system voltage stability.

A third and final test situation was developed to extend the robust simulation method to a larger and real case medium voltage network. In this case, approximation techniques were incorporated into the algorithm to reduce the computational complexity of the problem. The results showed that these approximations introduced only a small degree of conservativeness, as they include points in the forward reachable sets that are not actually attainable. Nevertheless, they allowed the robust simulation to run significantly faster. Results obtained on stability were consistent with the previous situation. Furthermore, by analyzing the forward propagated sets of an unstable network, it was possible to gain insights into how the network could be stabilized, for example, by decreasing the droop values of specific VC.

5.2 Future Work

This thesis explored the problem of voltage control interactions arising from the growing number of control devices integrated into active DN. In particular, it focused on VC, devices capable of regulating the reactive power injected at a node and adjusting active power injection when connected to a DER. As DNs evolve toward increasingly active and decentralized operation, network operators must ensure the stability of interactions among multiple autonomous control devices deployed across the grid.

One of the main challenges ahead lies in analyzing and guaranteeing the stability of systems that combine different types of controllers, especially those capable of manipulating both voltage and power flow, such as Soft Open Points (SOP). A natural direction for future research is therefore the integration of SOP control modes into the PWA state-space framework developed in this work. Extending the model to capture the behavior and interactions of SOP would allow for a more comprehensive stability analysis of ADN.

Other important research paths include the following: (i) finding the best optimal control curve according to stability and reachability criteria; (ii) include on the proposed stability analysis delays on actuation from devices; and (iii) extend the stability analysis to transmission networks to mitigate the risk of future blackouts due to voltage interactions.

5.3 Research Acknowledgements

During the development of this master's thesis, I was funded by the ATE - Alliance for Energy Transition project (C644914747-00000023), supported by the European Union through Next Generation EU under the Plano de Recuperação e Resiliência (PRR). I express my sincere gratitude to these institutions for their support and funding.

The work developed in this thesis led to the preparation of a manuscript, which has been submitted to the International Journal of Electrical Power and Energy Systems and is currently under peer review [71].

Bibliography

[1] Y. N. Harari, *Sapiens: A Brief History of Humankind*. Random House, 2014.

[2] J. E. Hansen, M. Sato, A. Lacis, R. Ruedy, I. Tegen, and E. Matthews, “Climate forcings in the industrial era,” *Proceedings of the National Academy of Sciences*, vol. 95, no. 22, pp. 12 753–12 758, 1998, dOI: 10.1073/pnas.95.22.12753.

[3] S. Solomon, G.-K. Plattner, R. Knutti, and P. Friedlingstein, “Irreversible climate change due to carbon dioxide emissions,” *Proceedings of the national academy of sciences*, vol. 106, no. 6, pp. 1704–1709, 2009, dOI: 10.1073/pnas.0812721106.

[4] B. Gates, *How to Avoid a Climate Disaster*. Penguin Books LTD, 2021.

[5] United Nations, “United nations framework convention on climate change,” Treaty Series, New York, NY, p. 107, May 1992, adopted May 9, 1992.

[6] K. Protocol, “Kyoto protocol,” *UNFCCC Website. Available online: http://unfccc. int/kyoto_protocol/items/2830. php (accessed on 1 January 2011)*, pp. 230–240, 1997.

[7] P. Agreement, “Paris agreement,” in *report of the conference of the parties to the United Nations framework convention on climate change (21st session, 2015: Paris). Retrived December*, vol. 4, no. 2017. HeinOnline, 2015, p. 2.

[8] T. Bruckner, I. A. Bashmakov, Y. Mulugetta, H. Chum, A. De la Vega Navarro, J. Edmonds, A. Faaij, B. Fungtammasan, A. Garg, E. Hertwich *et al.*, “Energy systems,” 2014.

[9] E. Papadis and G. Tsatsaronis, “Challenges in the decarbonization of the energy sector,” *Energy*, vol. 205, p. 118025, 2020, dOI: 10.1016/j.energy.2020.118025.

[10] M. Ilic, J. W. Black, and M. Prica, “Distributed electric power systems of the future: Institutional and technological drivers for near-optimal performance,” *Electric Power Systems Research*, vol. 77, no. 9, pp. 1160–1177, 2007, dOI: 10.1016/j.epsr.2006.08.013.

[11] A. Haque, P. Nguyen, W. Kling, and F. Bliek, “Congestion management in smart distribution network,” in *2014 49th International Universities Power Engineering Conference (UPEC)*. IEEE, 2014, pp. 1–6, dOI: 10.1109/UPEC.2014.6934751.

[12] P. Mallet, P.-O. Granstrom, P. Hallberg, G. Lorenz, and P. Mandatova, “Power to the people!: European perspectives on the future of electric distribution,” *IEEE Power and Energy Magazine*, vol. 12, no. 2, pp. 51–64, 2014, dOI: 10.1109/MPE.2013.2294512.

[13] S. Koziel, M. D. Ilić, D. M. Ferreira, P. M. Carvalho, and P. Hilber, “Data strategy for active distribution networks: a framework to quantify data granularity impact on cyber-physical planning and operation,” *Sustainable Energy, Grids and Networks*, vol. 43, p. 101763, 2025, dOI: 10.1016/j.segan.2025.101763. [Online]. Available: https://www.sciencedirect.com/science/article/pii/S2352467725001456

[14] P. Srivastava, R. Haider, V. J. Nair, V. Venkataramanan, A. M. Annaswamy, and A. K. Srivastava, “Voltage regulation in distribution grids: A survey,” *Annual Reviews in Control*, vol. 55, pp. 165–181, 2023, dOI: 10.1016/j.arcontrol.2023.03.008.

[15] ENTSO-E, “Grid incident in spain and portugal on 28 april 2025: Ics investigation expert panel factual report,” European Network of Transmission System Operators for Electricity (ENTSO-E), Tech. Rep., Oct. 2025, factual Report. [Online]. Available: https://www.entsoe.eu/publications/blackout/28-april-2025-iberian-blackout/#Introduction

[16] el Economista. (2025, Oct.) Red eléctrica alerta a la cnmc del riesgo de apagones por los problemas de control de tensión. Accessed: 2025-10-21. [Online]. Available: https://www.eleconomista.es/energia/noticias/13584464/10/25/red-electrica-alerta-a-la-cnmc-del-riesgo-de-apagones-por-los-problemas-de-control-de-tension.html

[17] D. M. V. P. Ferreira, “State-estimation and control for congestion management in weakly monitored active distribution networks,” Ph.D. dissertation, IST, 2025, dOI: 10.13039/501100001871.

[18] H. Lin and P. J. Antsaklis, “Stability and stabilizability of switched linear systems: A survey of recent results,” *IEEE Transactions on Automatic Control*, vol. 54, no. 2, pp. 308–322, 2009, dOI: 10.1109/TAC.2008.2012009.

[19] D. M. V. P. Ferreira and P. M. S. Carvalho, “Stability analysis of local control interactions in active distribution networks,” in *2023 IEEE International Conference on Energy Technologies for Future Grids (ETFG)*, 2023, pp. 1–6, dOI: 10.1109/ETFG55873.2023.10407342.

[20] P. D. F. Ferreira, P. M. S. Carvalho, L. A. F. M. Ferreira, and M. D. Ilić, “Distributed energy resources integration challenges in low-voltage networks: Voltage control limitations and risk of cascading,” *IEEE Transactions on Sustainable Energy*, vol. 4, no. 1, pp. 82–88, 2012, dOI: 10.1109/TSTE.2012.2201512.

[21] W. D. Stevenson *et al.*, *Elements of power system analysis*. McGraw-Hill New York, 1982, vol. 4.

[22] M. Baran and F. Wu, “Optimal capacitor placement on radial distribution systems,” *IEEE Transactions on Power Delivery*, vol. 4, no. 1, pp. 725–734, 1989, dOI: 10.1109/61.19265.

[23] N. G. Hingorani, “Flexible ac transmission,” *IEEE spectrum*, vol. 30, no. 4, pp. 40–45, 1993.

[24] A. Kulmala, S. Repo, and P. Järventausta, “Coordinated voltage control in distribution networks including several distributed energy resources,” *IEEE Transactions on Smart Grid*, vol. 5, no. 4, pp. 2010–2020, 2014, dOI: 10.1109/TSG.2014.2297971.

[25] W. Murray, M. Adonis, and A. Raji, “Voltage control in future electrical distribution networks,” *Renewable and sustainable energy reviews*, vol. 146, p. 111100, 2021, dOI: 10.1016/j.rser.2021.111100.

[26] E. Lakervi and E. J. Holmes, *Electricity distribution network design*. IET, 1995, no. 212.

[27] S. Corsi, M. Pozzi, C. Sabelli, and A. Serrani, “The coordinated automatic voltage control of the italian transmission grid-part i: reasons of the choice and overview of the consolidated hierarchical system,” *IEEE Transactions on power systems*, vol. 19, no. 4, pp. 1723–1732, 2004, dOI: 10.1109/TPWRS.2004.836185.

[28] D. M. V. P. Ferreira and P. M. S. Carvalho, “Setpoint reachability for congestion management in active distribution networks,” in *2024 International Conference on Smart Energy Systems and Technologies (SEST)*, 2024, pp. 1–6, dOI: 10.1109/SEST61601.2024.10694120.

[29] D. M. Ferreira and P. M. Carvalho, “State estimation in weakly monitored active distribution networks: Modeling soft open points functional behavior,” *Sustainable Energy, Grids and Networks*, vol. 33, p. 100967, 2023, dOI: 10.1016/j.segan.2022.100967.

[30] D. M. V. P. Ferreira, P. M. S. Carvalho, and L. A. F. M. Ferreira, “Optimal meter placement in low observability distribution networks with DER,” *Electric Power Systems Research*, vol. 189, p. 106707, 2020, dOI: 10.1016/j.epsr.2020.106707.

[31] K. Baker, A. Bernstein, E. Dall’Anese, and C. Zhao, “Network-cognizant voltage droop control for distribution grids,” *IEEE Transactions on Power Systems*, vol. 33, no. 2, pp. 2098–2108, 2017, dOI: 10.1109/TPWRS.2017.2735379.

[32] P. M. S. Carvalho, L. A. F. M. Ferreira, J. C. Botas, M. D. Ilic, X. Miao, and K. D. Bachovchin, "Ultimate limits to the fully decentralized power inverter control in distribution grids," in *2016 Power Systems Computation Conference (PSCC)*, 2016, pp. 1–7, dOI: 10.1109/PSCC.2016.7540893.

[33] K. Xiong, D. Cao, G. Zhang, Z. Chen, and W. Hu, "Coordinated Volt/VAR control for photovoltaic inverters: A soft actor-critic enhanced droop control approach," *International Journal of Electrical Power & Energy Systems*, vol. 149, p. 109019, 2023, dOI: 10.1016/j.ijepes.2023.109019.

[34] K. E. Antoniadou-Plytaria, I. N. Kouveliotis-Lysikatos, P. S. Georgilakis, and N. D. Hatziargyriou, "Distributed and decentralized voltage control of smart distribution networks: Models, methods, and future research," *IEEE Transactions on Smart Grid*, vol. 8, no. 6, pp. 2999–3008, 2017, dOI: 10.1109/TSG.2017.2679238.

[35] S. Bolognani, R. Carli, G. Cavraro, and S. Zampieri, "On the need for communication for voltage regulation of power distribution grids," *IEEE Transactions on Control of Network Systems*, vol. 6, no. 3, pp. 1111–1123, 2019.

[36] S. Weckx, C. Gonzalez, and J. Driesen, "Combined central and local active and reactive power control of pv inverters," *IEEE Transactions on Sustainable Energy*, vol. 5, no. 3, pp. 776–784, 2014, dOI: 10.1109/TSTE.2014.2300934.

[37] G. Valverde and T. Van Cutsem, "Model predictive control of voltages in active distribution networks," *IEEE Transactions on Smart Grid*, vol. 4, no. 4, pp. 2152–2161, 2013.

[38] P. Kundur, J. Paserba, V. Ajjarapu, G. Andersson, A. Bose, C. Canizares, N. Hatziargyriou, D. Hill, A. Stankovic, C. Taylor *et al.*, "Definition and classification of power system stability IEEE/CIGRE joint task force on stability terms and definitions," *IEEE transactions on Power Systems*, vol. 19, no. 3, pp. 1387–1401, 2004, dOI: 10.1109/TPWRS.2004.825981.

[39] M. Lundberg, O. Samuelsson, and E. Hillberg, "Local voltage control in distribution networks using PI control of active and reactive power," *Electric Power Systems Research*, vol. 212, p. 108475, 2022, dOI: 10.1016/j.epsr.2022.108475.

[40] A. Eggli, S. Karagiannopoulos, S. Bolognani, and G. Hug, "Stability analysis and design of local control schemes in active distribution grids," *IEEE Transactions on Power Systems*, vol. 36, no. 3, pp. 1900–1909, 2021, dOI: 10.1109/TPWRS.2020.3026448.

[41] J. Schmitt, S. Ecklebe, S. Krahmer, K. Roebenack, and P. Schegner, "An extended stability criterion for grids with Q(V)-controlled distributed energy resources," in *PESS 2023; Power and Energy Student Summit*, 2023, pp. 7–12.

[42] X. Zhou, J. Tian, L. Chen, and E. Dall'Anese, "Local voltage control in distribution networks: A game-theoretic perspective," in *2016 North American Power Symposium (NAPS)*. IEEE, 2016, pp. 1–6, dOI: 10.1109/NAPS.2016.7747940.

[43] R. Goebel, R. G. Sanfelice, and A. R. Teel, "Hybrid dynamical systems," *IEEE control systems magazine*, vol. 29, no. 2, pp. 28–93, 2009.

[44] E. Sontag, "Nonlinear regulation: The piecewise linear approach," *IEEE Transactions on automatic control*, vol. 26, no. 2, pp. 346–358, 1981, dOI: 10.1109/TAC.1981.1102596.

[45] C. D. Toth, J. O'Rourke, and J. E. Goodman, *Handbook of discrete and computational geometry*. CRC press, 2017.

[46] F. Borrelli, A. Bemporad, and M. Morari, *Predictive Control for Linear and Hybrid Systems*. Cambridge University Press, 2017.

[47] A.-A. Fouad and V. Vittal, *Power system transient stability analysis using the transient energy function method*. Pearson Education, 1991.

[48] S. Boyd, L. El Ghaoui, E. Feron, and V. Balakrishnan, *Linear matrix inequalities in system and control theory*. SIAM, 1994.

[49] M. K.-J. Johansson, *Piecewise linear control systems: a computational approach*. Springer, 2003, vol. 284.

[50] D. Mignone, G. Ferrari-Trecate, and M. Morari, "Stability and stabilization of piecewise affine and hybrid systems: an lmi approach," in *Proceedings of the 39th IEEE Conference on Decision and Control (Cat. No.00CH37187)*, vol. 1, 2000, pp. 504–509 vol.1.

[51] R. A. DeCarlo, M. S. Branicky, S. Pettersson, and B. Lennartson, "Perspectives and results on the stability and stabilizability of hybrid systems," *Proceedings of the IEEE*, vol. 88, no. 7, pp. 1069–1082, 2000, dOI: 10.1109/5.871309.

[52] G. Feng, "Stability analysis of piecewise discrete-time linear systems," *IEEE Transactions on Automatic Control*, vol. 47, no. 7, pp. 1108–1112, 2002, dOI: 10.1109/TAC.2002.800666.

[53] J. LaSalle, "Some extensions of liapunov's second method," *IRE Transactions on circuit theory*, vol. 7, no. 4, pp. 520–527, 1960, dOI: 10.1109/TCT.1960.1086720.

[54] P. Biswas, P. Grieder, J. Löfberg, and M. Morari, "A survey on stability analysis of discrete-time piecewise affine systems," *IFAC Proceedings Volumes*, vol. 38, no. 1, pp. 283–294, 2005, dOI: 10.3182/20050703-6-CZ-1902.00332.

[55] M. Kantner, “Robust stability of piecewise linear discrete time systems,” in *Proceedings of the 1997 American Control Conference (Cat. No. 97CH36041)*, vol. 2. IEEE, 1997, pp. 1241–1245, dOI: 10.1109/ACC.1997.609732.

[56] M. Kantner and J. Doyle, “Robust simulation and nonlinear performance,” in *Proceedings of 35th IEEE Conference on Decision and Control*, vol. 3. IEEE, 1996, pp. 2622–2623, dOI: 10.1109/CDC.1996.573498.

[57] A. El-Guindy, D. Han, and M. Althoff, “Estimating the region of attraction via forward reachable sets,” in *2017 American Control Conference (ACC)*. IEEE, 2017, pp. 1263–1270, dOI: 10.23919/ACC.2017.7963126.

[58] A. Bemporad, F. D. Torrisi, and M. Morari, “Optimization-based verification and stability characterization of piecewise affine and hybrid systems,” in *International Workshop on Hybrid Systems: Computation and Control*. Springer, 2000, pp. 45–58.

[59] A. Bemporad, C. Filippi, and F. D. Torrisi, “Inner and outer approximations of polytopes using boxes,” *Computational Geometry*, vol. 27, no. 2, pp. 151–178, 2004, dOI: 10.1016/S0925-7721(03)00048-8.

[60] European Commission, “Commission regulation (eu) 2016/631 of 14 april 2016 establishing a network code on requirements for grid connection of generators (text with eea relevance),” 2016. [Online]. Available: http://data.europa.eu/eli/reg/2016/631/oj

[61] Ministério do Ambiente e Ação Climática, “Portaria n.º 73/2020 de 16 de março,” 2020, diário da República, 1.ª série, N.º 53, 16 de março de 2020, p. 39. [Online]. Available: https://dre.pt/dre/detalhe/portaria/73-2020-130225698

[62] Comisión Nacional de los Mercados y la Competencia, “Resolución de 12 de junio de 2025, de la Comisión Nacional de los Mercados y la Competencia, por la que se modifican los procedimientos de operación para el desarrollo de un servicio de control de tensión en el sistema eléctrico peninsular español,” Boletín Oficial del Estado, núm. 153, 26 de junio de 2025, pp. 84733–84873, 2025, Sección III: Otras disposiciones. Referencia BOE-A-2025-13076. [Online]. Available: https://www.boe.es/diario_boe/txt.php?id=BOE-A-2025-13076

[63] “IEEE standard for interconnection and interoperability of distributed energy resources with associated electric power systems interfaces,” *IEEE Std 1547-2018 (Revision of IEEE Std 1547-2003)*, pp. 1–138, 2018, dOI: 10.1109/IEEESTD.2018.8332112.

[64] P. Radatz, M. Rylander, A. Huque, J. Vaz, A. Alrifai, S. Arafa, and R. Ruvini, “Tailoring IEEE 1547 recommended smart inverter settings based on modeled grid performance,” Electric Power Re-

search Institute (EPRI), Palo Alto, CA, Tech. Rep. 11317449, December 2020, national Grid Solar Phase II Program Report.

[65] J. M. Bloemink and T. C. Green, “Benefits of distribution-level power electronics for supporting distributed generation growth,” *IEEE Transactions on Power Delivery*, vol. 28, no. 2, pp. 911–919, 2013, dOI: 10.1109/TPWRD.2012.2232313.

[66] J. Yang, N. Zhang, C. Kang, and Q. Xia, “A state-independent linear power flow model with accurate estimation of voltage magnitude,” *IEEE Transactions on Power Systems*, vol. 32, no. 5, pp. 3607–3617, 2016, dOI: 10.1109/TPWRS.2016.2638923.

[67] D. M. Ferreira, P. M. Carvalho, and M. D. Ilić, “A kalman filter approach for state estimation in weakly monitored active distribution networks,” *Sustainable Energy, Grids and Networks*, vol. 39, p. 101423, 2024, dOI: 10.1016/j.segan.2024.101423. [Online]. Available: https://www.sciencedirect.com/science/article/pii/S2352467724001528

[68] P. C. Leal, D. M. V. P. Ferreira, and P. M. S. Carvalho, “Data analytics for admittance matrix estimation of poorly monitored distribution grids,” *Energies*, vol. 15, no. 23, 2022, dOI: 10.3390/en15238961. [Online]. Available: https://www.mdpi.com/1996-1073/15/23/8961

[69] S. S. Guggilam, E. Dall’Anese, Y. C. Chen, S. V. Dhople, and G. B. Giannakis, “Scalable optimization methods for distribution networks with high pv integration,” *IEEE Transactions on Smart Grid*, vol. 7, no. 4, pp. 2061–2070, 2016, dOI: 10.1109/TSG.2016.2543264.

[70] J. Lofberg, “Yalmip : a toolbox for modeling and optimization in matlab,” in *2004 IEEE International Conference on Robotics and Automation (IEEE Cat. No.04CH37508)*, 2004, pp. 284–289, dOI: 10.1109/CACSD.2004.1393890.

[71] T. G. Glória, D. M. V. P. Ferreira, F. Steinke, and P. M. S. Carvalho, “Stability of voltage control interactions in active distribution networks: An approach for local PI-controllers with piecewise-linear control laws,” *International Journal of Electrical Power and Energy Systems*, 2025, (Under review).

A

IEEE Volt/VAr Curves default parameters

Voltage-reactive power parameters	**Default settings**		**Ranges of allowable settings**	
	Category A	**Category B**	**Minimum**	**Maximum**
V_{ref}	V_N	V_N	$0.95V_N$	$1.05V_N$
V_2	V_N	$V_{ref} - 0.02\,V_N$	A: V_{ref} B: $V_{ref} - 0.03V_N$	V_{ref}
Q_2	0	0	100% of nameplate reactive power capability, absorption	100% of nameplate reactive power capability, injection
V_3	V_N	$V_{\text{ref}} + 0.02\,V_N$	V_{ref}	Category A: V_{ref} Category B: $V_{\text{ref}} + 0.03\,V_N$
Q_3	0	0	100% of nameplate reactive power capability, absorption	100% of nameplate reactive power capability, injection
V_1	$0.9\,V_N$	$V_N - 0.08\,V_N$	$V_{\text{ref}} - 0.18\,V_N$	$V_2 - 0.02\,V_N$
Q_1[a]	25% of nameplate apparent power rating, injection	44% of nameplate apparent power rating, injection	0	100% of nameplate reactive power capability, injection[b]
V_4	$1.1\,V_N$	$V_N + 0.08\,V_N$	$V_3 + 0.02\,V_N$[c]	$V_{\text{ref}} + 0.18\,V_N$
Q_4	25% of nameplate apparent power rating, absorption	44% of nameplate apparent power rating, absorption	100% of nameplate reactive power capability, absorption	0
Open loop response time	10 s	5 s	1 s	90 s

Table A.1: Voltage-reactive power parameters and their default settings and allowable ranges [63].